NeuroImage 274 (2023) 120144

Contents lists available at ScienceDirect

NeuroImage

journal homepage: www.elsevier.com/locate/neuroimage

Getting off track: Cortical feedback processing network modulated by continuous error signal during target-feedback mismatch

Hannah S. Pulferer[a], Kyriaki Kostoglou[a], Gernot R. Müller-Putz[a,b,*]

[a] Institute of Neural Engineering, Graz University of Technology, Stremayrgasse 16/IV, Graz, Austria
[b] BioTechMed-Graz, Graz, Austria

ARTICLE INFO

Keywords:
Electroencephalography (EEG)
Continuous error processing
Feedback processing
Corrective behavior
Spinal cord injury
Error-related negativity (ERN)
Feedback-related negativity (FRN)
Error positivity (Pe)

ABSTRACT

Performance monitoring and feedback processing – especially in the wake of erroneous outcomes – represent a crucial aspect of everyday life, allowing us to deal with imminent threats in the short term but also promoting necessary behavioral adjustments in the long term to avoid future conflicts. Over the last thirty years, research extensively analyzed the neural correlates of processing discrete error stimuli, unveiling the error-related negativity (ERN) and error positivity (Pe) as two main components of the cognitive response. However, the connection between the ERN/Pe and distinct stages of error processing, ranging from action monitoring to subsequent corrective behavior, remains ambiguous. Furthermore, mundane actions such as steering a vehicle already transgress the scope of discrete erroneous events and demand fine-tuned feedback control, and thus, the processing of continuous error signals – a topic scarcely researched at present. We analyzed two electroencephalography datasets to investigate the processing of continuous erroneous signals during a target tracking task, employing feedback in various levels and modalities. We observed significant differences between correct (slightly delayed) and erroneous feedback conditions in the larger one of the two datasets that we analyzed, both in sensor and source space. Furthermore, we found strong error-induced modulations that appeared consistent across datasets and error conditions, indicating a clear order of engagement of specific brain regions that correspond to individual components of error processing.

1. Introduction

From a young age, our abilities to monitor our surroundings and distinguish intended from actual decision outcomes define our success in everyday life. Certainly, challenging situations may require an adequate on-the-fly change of plan to reconcile previous expectations with observed results and to subsequently ensure success in the short term (Rabbitt, 1966). Yet, apart from the immediate benefits of flexibly adapting our modus operandi, the capability of closely monitoring our actions, and more importantly, of recognizing possibly problematic consequences of our approach, entails crucial advantages in the long run as well (Ullsperger et al., 2014). As our actions force specific results, we acquire often highly versatile mappings between specific actions and their outcomes (Lourenco and Casey, 2013). In order to optimize these action-outcome mappings towards optimal behavior for a specific situation, an intuition about when to adapt our behavior and when to remain firm in our approach - in short, an awareness of erroneous versus correct responses - is essential (van der Helden et al., 2009). As a result, an in-depth understanding of feedback processing, especially regarding erroneous feedback, is vital to gain insights on how the brain adapts to a dynamic environment and thus enables behavioral adjustments and learning.

1.1. Cognitive processing of discrete error stimuli and behavioral adjustments

Previous research extensively investigated how the human brain reacts to discrete erroneous stimuli by means of noninvasive recordings such as the electroencephalogram (EEG). Usually elicited within Stroop (Olvet and Hajcak, 2008), Flanker (Ullsperger and Szymanowski, 2004), or simple Go/No-Go tasks (Falkenstein et al., 2000), the error-related negativity (ERN) quickly emerged as one of the most prominent neural correlates to error processing. Argued to arise in the dorsal anterior cingulate cortex (ACC) (Dehaene et al., 1994; Mathewson et al., 2005), the ERN (often referred to as response ERN) is mainly characterized by its fronto-central negativity in the topography of the EEG approximately 100 ms after the onset of an erroneous stimulus, and proved to be robust to both differing error modalities (Holroyd et al., 1998; Van 't Ent and Apkarian, 1999) and stimulus types (Miltner et al., 1997). A special instance of the ERN, the feedback ERN, shares the

* Corresponding author.
E-mail address: gernot.mueller@tugraz.at (G.R. Müller-Putz).

https://doi.org/10.1016/j.neuroimage.2023.120144.
Received 13 October 2022; Received in revised form 14 April 2023; Accepted 27 April 2023
Available online 28 April 2023.

same physiology, but arises with a latency of around 250 ms after a feedback stimulus signaling a transpired error (Miltner et al., 1997; Badgaiyan and Posner, 1998; Nieuwenhuis et al., 2004); as such, this specific correlate gained special attention in relation to action monitoring and feedback processing (Ullsperger et al., 2014). While competing theories suggest a functional significance in connection to either error detection (Falkenstein et al.), conflict monitoring (Carter et al., 1998; Botvinick et al., 2001; Yeung et al., 2004), or reinforcement learning (Holroyd and Coles, 2002), all leading views relate the ERN to a comparison process between intended and observed outcomes at a fundamental level. However, of these theories, reinforcement learning in particular suggests a clear connection between the classical response ERN, the feedback ERN, and learning. Specifically, in an early phase of training – and hence in the absence of proficient internal judgment of the current performance – learning relies exclusively on external feedback and thus leads to initially large feedback ERNs and an absence of internally-informed response ERNs. With learning, a mapping between input and correct output subsequently forms, and the feedback ERN diminishes as the response ERN increases (Holroyd and Coles, 2002). In short, there will be no need to rely on feedback once we now right from wrong by ourselves; a hypothesis that has been both confirmed (van der Helden et al., 2009) and questioned (Nieuwenhuis et al., 2002), leaving mixed evidence on a clear relation between the ERN, feedback processing and remedial behavior in response to errors. However, ERN durations and amplitudes covarying with the duration until an error correction takes place nonetheless imply an important role in corrective behavior following error detection (Burle et al., 2008; Gehring et al., 2012).

In contrast to the automated nature of the ERN, yet another well-researched correlate in the context of error processing – the error positivity (Pe) – reportedly traces conscious error perception and remedial action following faulty performance (Nieuwenhuis et al., 2001; Endrass et al., 2007). While the ERN exhibits a stationary course for both aware and unaware errors, the Pe, characterized by a centro-parietal positive deflection in the EEG around 300–500 ms after an error onset, clearly modulates with error awareness (Nieuwenhuis et al., 2001). Previous work for instance linked Pe amplitudes to an accumulation of evidence in error detection (Steinhauser and Yeung, 2010), as well as confidence in decision-making (Boldt and Yeung, 2015), which was in turn suggested as a vital part of performance monitoring and demonstrated considerable impact on behavioral adaptations and learning (Frömer et al., 2021). Additional studies suggested a further relation between the Pe and strategic behavioral adjustments such as post-error improvements in accuracy (Carp and Compton, 2009) and post-error slowing (Chang et al., 2014), further stressing its vital role in the conscious processing of errors and the long-term adaptations related to learning.

Overall, the characteristics of the mentioned correlates have been investigated in depth within previous research; however, a clear picture on the interplay between these correlates, and crucially, how they relate to and enforce behavioral adjustments and thus learning, remains unclear (Gehring et al., 2018).

1.2. Continuous feedback processing and corrective behavior

Many open questions in relation to error processing have been resolved since initial reports on the ERN (Falkenstein, 1989); however, research almost exclusively focused on the processing of discrete error stimuli in this context. Due to the nature of the observed correlates, it stands to reason that a binary approach in paradigm design – a clear ‘error’ or ‘no error’ trial structure - is the appropriate course of action. This has been further promoted by findings on the influence of error rates on the ERN; specifically, that large amounts of error trials within a paradigm attenuate the amplitudes of the recorded ERNs. Error-likelihood theory – yet another account based on the reinforcement learning view of error processing – incorporated this observation and proposed that neurons in the ACC learn to predict the likelihood of an occurring error in relation to a given task (Brown and Braver, 2005), which further restricted paradigm design in error processing research. Indeed, a focus on how the brain might process continuous instead of discrete deviations from an intended goal would imply an extended exposure to erroneous input signals, which, according to error-likelihood theory, would inherently lead to diminishing ACC activity and thus ERN amplitudes. However, moving on from laboratory conditions, a range of everyday-situations demands fine-tuned feedback-control rather than a coarse distinction between correct or wrong, which further encourages detailed research on the processing of continuous erroneous feedback signals in addition to the well-known discrete error stimuli. Frömer and colleagues recently raised the question of how the brain regulates remedial action and learning from new feedback-related information using the example of throwing darts and attempting to hit the bullseye; the corrections taking place after narrowly missing, in theory, should settle on a different scale than those after missing the board entirely (Frömer et al., 2021). While playing darts might not be of immediate importance to our daily routine, this line of thought can easily translate into the continuous adjustments necessary to, e.g., steer a car, which may similarly range from minute changes to considerable corrections in order to stay on course. How does the brain process continuous feedback regarding ongoing deviations from an intended target? How does this processing relate to an identification of erroneous outcomes and variable levels of corrections? And lastly, how do we selectively learn from processing continuous inputs?

In contrast to the error-likelihood theory, the before-mentioned theories promoting conflict monitoring and reinforcement-learning could in principle accommodate the continuous exposure to an erroneous signal. However, to the best of our knowledge, an explicit extension of the framework comprising the processing of discrete error stimuli towards continuous error signals has not been attempted for either of the theories surrounding the ERN and Pe. As a result, we argue that the investigation of erroneous feedback processing evoked by continuous error signals may enable an in-depth understanding not only of error processing, but corrective behavior and learning as well.

1.3. Rationale for the present study

Within this study, we addressed three major questions. First, is it even possible to measure the correlates of error processing from continuously varying erroneous feedback signals instead of discrete error stimuli? Separate groups tackled variations of this question already; however, their approaches largely based on the continuity of the task itself rather than the continuity of the erroneous input (Spüler and Niethammer, 2015; Lopes-Dias et al., 2018; Völker et al., 2018). Second, how do such continuously varying error signals affect different brain regions? Phase-locked cortical responses demonstrably arise, e.g., during periodic movement (Seeber et al., 2015); however, to our knowledge, modulations in error perception have not yet been investigated. Furthermore, reports suggest a large number of contributors to both the ERN and the Pe, ranging from the dorsal and rostral ACC to the Pre-supplementary motor area (Pre-SMA) and orbitofrontal cortex (OFC) (Herrmann et al., 2004; Turken and Swick, 2008); nonetheless, a conclusive theory on the individual role or the interplay between these regions is still missing. And third, is there a clear connection between the ERN, the Pe, and corrective behavior? If we define ‘error processing’ as a combination of subprocesses, various cortical networks direct each distinct part. However, owing to unintuitive ‘button-pressing tasks’ described by Gehring and colleagues, a unifying theory explaining naturalistic error-and-correction behavior remains desirable (Gehring et al., 2018).

To answer these questions, we investigated two pre-recorded datasets employing motor attempt and motor execution that shared the same paradigm. These datasets comprise forty sessions of electroencephalographic (EEG) recordings in twenty able-bodied participants (preliminary analysis published in (Pulferer and Müller-Putz, 2022)). To obtain further insight into the elicited cortical processes independent of

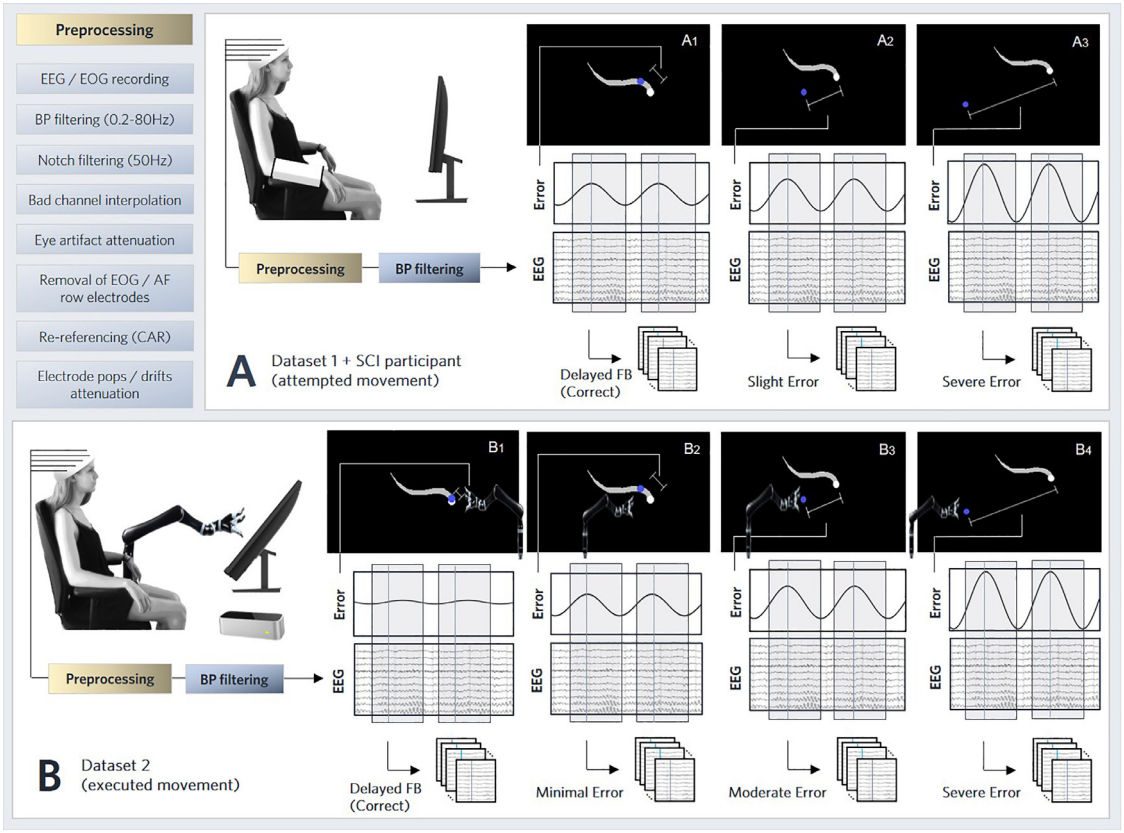

Fig. 1. Data preprocessing pipeline and analysis scheme for all discussed datasets. **A Dataset 1/participant with SCI**. An encasing around the dominant arm prevented overt movement, target (white snake) and feedback (blue dot) were presented strictly on-screen. Delayed feedback (correct) was delivered during the calibration part (**A1**), which was then gradually replaced by first 50% (**A2**) and finally 100% (**A3**) EEG-decoded positional information. **B Dataset 2**. The participants' unrestrained dominant arm movement was recorded via LeapMotion, and direct feedback was delivered via an assistive robotic arm. During calibration, hand movement was directly fed to the robot (**B1**). This direct control was gradually replaced by first 33% (**B2**), then 66% (**B3**), and finally 100% (**B4**) EEG-decoded positional information. For all datasets, processed data were band-pass filtered in 12 bands of interest and epoched within [−1,3]s of local maxima of the Euclidean error signal between the positions of target (snake) and feedback (Dataset 1/participant with SCI: feedback dot, Dataset 2: robotic arm).

any afferent input related to the specific movement task, we additionally analyzed one session in a participant with cervical spinal cord injury (SCI). During each session, the participants underwent a continuous target tracking task in two dimensions (2D), employing various levels of correct and increasingly erroneous feedback. For lack of pre-defined error stimuli within this continuous setup, we chose to time-lock the data to local maxima of the Euclidean error signal between target and feedback. We hypothesized that with an increasing mismatch between target and feedback, increasing activation of brain regions involved in error processing should arise.

2. Materials and methods

We performed offline analyses on two different pre-recorded EEG datasets, comprising data of 20 able-bodied participants, as well as one person with SCI, in a total of 41 sessions of recordings. Both studies initially investigated continuous 2D movement decoding and constitute consecutive parts of the "Feel Your Reach" project (Müller-Putz et al., 2022). As such, they broadly share a common target tracking task with different feedback conditions, respectively (see Fig. 1). The paradigm was implemented using MATLAB (MATLAB 2015b, MathWorks Inc. USA) and Psychtoolbox (Brainard, 1997; Pelli, 1997; Kleiner et al., 2007). We recorded and synchronized all data via lab streaming layer (https://github.com/sccn/labstreaminglayer). Both studies took place at the Graz University of Technology following approval by the ethics committee of the Medical University of Graz (votum number 32–583 ex 19/20). Participants gave their written informed consent and received monetary compensation for their time. The raw EEG datasets as well as related Matlab scripts are available upon request to the corresponding author and require a formal data sharing agreement.

2.1. Dataset description

2.1.1. Dataset 1

Dataset 1 corresponds to EEG signals of ten right-handed (Oldfield, 1971) participants (24 (mean) ± 5 (SD) years, five male) in three sessions each recorded within a prior study (Pulferer et al., 2022), amounting to a total of 30 recorded sessions. The setup consisted of 64 active electrodes (actiCAP, Brain Products GmbH, Gilching, Germany), comprising a 60-channel EEG and 4-channel electrooculogram (EOG) at a sampling rate of 200 Hz. The mounting of the EEG channels obeyed the international 10–10 system (see Fig.S1, supplementary material), with slight modifications to allocate four electrodes to the EOG and facilitate increased signal density in the parieto-occipital area, a region of particular importance in visuomotor tasks (Wenderoth et al., 2005; Mulliken et al., 2008). To monitor saccades and blinks, we placed EOG electrodes at the outer canthi of both eyes, and above and below the left eye. The study initially served to investigate the effects of user training across identical sessions of a 2D target tracking task utilizing **attempted movement** (Müller-Putz et al., 2016; Chen et al., 2021). We chose this dataset due to the limited performance of the decoder, which led to periodically varying levels of feedback-target-deviation and thus facilitated the analysis of continuously varying feedback processing.

2.1.2. Dataset 2

Dataset 2 comprises 64-channel EEG and 6-channel EOG recordings of ten participants (27 (mean) ± 4 (SD) years, five male, one left-handed), one session each (an therefore a total of 10 sessions), sampled at 500 Hz (Mondini et al., 2020). In addition to the EOG setup of Dataset 1, two more EOG electrodes were placed at the inner canthi of both eyes. As we recorded Dataset 2 before Dataset 1, wherein we optimized the electrode setup regarding visuomotor tasks as previously described, signals acquired in Dataset 2 corresponded to the standard 10–10 system without further modifications. Dataset 2 initially served to investigate the feasibility of continuous online decoding of **executed arm movements** in 2D, and was chosen as a complementary dataset to Dataset 1 as they shared the same paradigm, providing largely the same structure within and between single runs, and thus allowing an identical analysis scheme. However, the different control modes of attempted movement (Dataset 1) and executed movement (Dataset 2) provided the possibility of strengthening our hypothesis that the observed effects pertain primarily to error and feedback processing, disregarding the mode of control.

2.1.3. Participant with SCI

Following a similar line of thought and benefitting from the shared paradigm once more, we additionally analyzed data previously recorded from a participant with SCI (Pulferer et al., 2022) to further investigate both the characteristics of feedback processing, and the arising corrective mechanisms, in persons with limited motor output. The participant (male, 36) experienced a traumatic complete spinal cord injury (SCI) at the neurological level of injury (NLI) C2 in 2003 as a result of a motorbike accident (AIS A, (Maynard et al., 1997)), leading to a complete loss of motor output and sensory impression from the neck downwards, and necessitating artificial ventilation. In terms of paradigm, the participant with SCI completed the same task as all able-bodied participants recorded within Dataset 1. This entailed the same target tracking task utilizing **attempted movement** of his previously dominant (right) arm, with feedback presented strictly on-screen via feedback dot. The recordings corresponded to the 60-channel EEG and 4-channel EOG setup described in 2.1.1. Dataset 1, sampled at 200 Hz. For data processing and analysis, both in sensor as well as in source space, the same procedures as described for able-bodied participants were employed here as well. However, due to sporadic muscle contractions in the neck area, we chose to bandpass filter the data exclusively in the delta band (0.2–4 Hz) to avoid excessive contamination due to muscle artifacts.

2.2. Experimental design and setup

For both datasets, each session of recordings included an offline calibration part, implemented for data acquisition to train a movement decoder (Kobler et al., 2020; Martinez-Cagigal et al., 2020), and a subsequent online part, during which the trained decoder delivered real-time-decoded positional feedback.

2.2.1. Dataset 1

For sessions of Dataset 1, participants sat in front of a TV screen (46 inches) and had to track the target (white snake) via **attempted movement** of their dominant arm as if wielding a computer mouse (Fig. 1A). We chose this task type since participants reported a more intuitive perception of attempted movement than in motor imagery (Ofner et al., 2017; Chen et al., 2021). An encasing around the limb prevented overt movement, mimicking the restrictions experienced by persons with limitations in motor control. For Dataset 1, one session consisted of 10 runs containing 12 trials each, with a tracking sequence of 23 s duration per trial. During calibration (Fig. 1A1, four runs), a blue feedback dot on the screen depicted largely correct feedback (a slightly delayed snake) to get the participants accustomed to the additional visual information before actual online feedback was delivered during the online part. Aside from the delay of the feedback dot, feedback and target coincided during the calibration runs, leading to our hypothesis that no error processing arose during calibration runs. We henceforth term epochs of calibration data '*Delayed Feedback*'. Within the online part, we first displayed feedback corresponding to only 50% of the EEG-decoded information by depicting the arithmetic mean between actual and decoded target positions. This incremental increase of EEG-decoded positional information was utilized to slowly prepare the participants for the potentially erroneous online decoding (Fig. 1A2, three runs). As the decoding performance worsened compared to the calibration runs (offering the slightly delayed correct feedback), we hypothesized that erroneous feedback processing had to arise within the 50% EEG-decoded feedback runs, and thus henceforth label epochs of 50% EEG-decoded feedback as '*Slight Error*'. Finally, we disregarded the actual target positions completely and exclusively displayed 100% of the EEG-decoded positional information (Fig. 1A3, three runs). Again, the decoding performance worsened with respect to the previously depicted 50% EEG-decoded feedback runs, and we hypothesized that within the 100% EEG-decoded feedback runs, erroneous feedback processing had to reach a maximum for our paradigm. Thus, we henceforth label epochs of 100% EEG-decoded feedback '*Severe Error*'. For all conditions, including the fake feedback condition during calibration, the participants were explicitly instructed about the nature of the specific feedback.

2.2.2. Dataset 2

During each recording session of Dataset 2, participants had to track a moving target (white snake) on a reclined screen (46 inches) by **executing movement** with their dominant arm as we recorded EEG signals (Fig. 1B). In contrast to measurements of Dataset 1, a LeapMotion controller (LeapMotion Inc., USA) collected the kinematics of this tracking movement while an assistive robotic arm (JACO, Kinova Robotics Inc, Canada) delivered real-time feedback in front of the screen, as opposed to the strictly on-screen feedback employed for Dataset 1. For Dataset 2, one session consisted of 11 runs containing 12 trials each, with a tracking sequence of 23 s duration per trial. During calibration (Fig. 1B1, five runs), we directly reproduced the movement information recorded by the LeapMotion with the robotic arm, leading to feedback that corresponded exactly to the self-controlled arm movement of the participants with a slight time delay. Since the participants thus had full control over the robot during calibration, feedback and target coincided, implying that no error processing arose. As in Dataset 1, we term epochs of calibration data *'Delayed Feedback'* henceforth. Within the online part, we again slowly accustomed the participants to the increasingly erroneous EEG-decoded positional information; however, as opposed to Dataset 1, we displayed two transitional feedback conditions instead of only one before presenting the fully EEG-decoded feedback. First, we displayed a mixture of 33% EEG-decoded positional information and 66% LeapMotion-recorded actual hand positions (Fig. 1B2, two runs). The incremental transition from arm-controlled to EEG-decoded positional information induced an increasing perceived deviation of the feedback from the target, again leading to our hypothesis that erroneous feedback processing increased steadily during the online part of the measurement. We thus term epochs featuring 33% EEG-decoded positional information *'Minimal Error'* henceforth. Subsequently, we increased the EEG-decoded positional information to 66% (see Fig. 1B3, two runs), thus reducing the LeapMotion-recorded positional information to only 33%. In the following, epochs corresponding to 66% EEG-decoded positional information are termed *'Moderate Error'*. And finally, we exclusively displayed 100% EEG-decoded positional information (see Fig. 1B4, two runs). Hypothesizing that during this last online condition a maximum in feedback processing had to arise, we henceforth label epochs featuring 100% EEG-decoded positional information *'Severe Error'*, matching with Dataset 1. Due to the different incremental increases of EEG-decoded positional information in Datasets 1 and 2, only the Delayed Feedback and Severe Error conditions directly match across datasets; however, we nevertheless included the transition runs in our analysis (50% EEG-decoded for Dataset 1, 33% and 66% EEG-decoded for Dataset 2) to gain an understanding of feedback processing across various levels of performance.

Table 1
Overview of the specifics of all analyzed datasets.

	Dataset 1	Dataset 2	Spinal cord injured participant
Participants / Age	10 / (24 ± 5) ys	10 / (27 ± 4) ys	36 ys (NLI C2, AIS A)
Sessions in Total	30 (i.e., 3 sessions per participant)	10 (i.e., 1 session per participant)	1
Trials in Total	3600 (at 23 s)	1320 (at 23 s)	96 (at 23 s)
Mean Epochs/Trial	6.3	8.0	6.1
Gender	5 male	5 male	male
Handedness	all right-handed	one left-handed	previously right-handed
Sampling Rate	200 Hz	500 Hz	200 Hz
EEG Recordings	60-channel (modified 10–10 system)	64-channel (standard 10–10 system)	60-channel (modified 10–10 system)
EOG Recordings	4-channel	6-channel	4-channel
Task Type	attempted movement	executed movement	attempted movement
Feedback *(Calibration part)*	- delayed feedback (delayed snake) (4 runs)	- user hand kinematics (recorded via LeapMotion) (5 runs)	- delayed feedback (delayed snake) (4 runs)
Feedback *(Online part)*	- 50% EEG-decoded - 100% EEG-decoded (3 runs each)	- 33% EEG-decoded - 66% EEG-decoded - 100% EEG-decoded (2 runs each)	- 50% EEG-decoded - 100% EEG-decoded (2 runs each)
Feedback Modality	strictly on-screen feedback	assistive robotic arm (JACO)	strictly on-screen feedback

Table 2
Frequency bands of interest.

Frequency band	Delta	Theta	Alpha	Beta	Gamma 1	Gamma 2	Gamma 3	Gamma 4	Gamma 5	Low	High	Broad
Range (Hz)	0.2–4	4–8	8–13	13–30	30–40	40–50	50–60	60–70	70–80	0.2–30	30–80	0.2–80

Similarly to Dataset 1, the participants included in Dataset 2 were explicitly instructed about the respective feedback conditions.

2.2.3. Participant with SCI

The measurement with the participant with SCI employed the same paradigm discussed for Dataset 1, i.e., an attempted movement task providing feedback in the form of a feedback dot on the TV screen. As in Dataset 1, four calibration runs (henceforth 'Delayed Feedback') depicting correct but slightly delayed feedback were recorded; however, due to the participant's long journey to join us at the laboratory, we only recorded two runs each for the 50% (henceforth 'Slight Error') and 100% (henceforth 'Severe Error') EEG-decoded feedback conditions.

Table 1 briefly summarizes the specifics of all investigated datasets.

2.3. Data preprocessing

The preprocessing pipeline illustrated in Fig. 1 depicts our data preprocessing approach. Both EEG and EOG data were first bandpass filtered between 0.2–80 Hz, and 50 Hz power line noise interference was removed using a notch filter.

Next, bad channels, as identified by visual inspection, were interpolated from their neighboring channels using spherical splines. As described in the original publications (Mondini et al., 2020; Pulferer et al., 2022), we trained an eye artifact subtraction model (Kobler et al., 2020a) to remove EEG components corresponding to saccadic eye movements and blinks. To minimize the further influence of eye movements on the EEG, EOG and anterior frontal (AF) row electrodes (i.e., the channels closest to the corneoretinal dipole) were subsequently removed. We further re-referenced all remaining channels to their common average and used the HEAR algorithm (Kobler et al., 2019) to attenuate pops and drifts in the data. Additionally, trials affected by other physiological artifacts (e.g., muscle artifacts) were identified by visual inspection and rejected from further analysis. After visual inspection, none of the epochs exceeded ±100 μV. Finally, Dataset 2 was downsampled to 200 Hz to match the sampling rate of Dataset 1. As the last step, data were zero-phase bandpass filtered into 12 bands of interest (see Table 2) using a 10th-order Butterworth filter. We chose these bands of interest on the basis of previous literature describing delta to beta bands (Yordanova et al., 2004; Koelewijn et al., 2008; Carp and Compton, 2009) as informative for error processing. In addition, a more recent work analyzed high-gamma activity during error processing (Völker et al., 2018), promoting the investigation of sub-bands of the gamma for our purposes. To finally scout for information relating to error and feedback processing in wider frequency ranges, we additionally considered frequency bands corresponding to the merged low (delta to beta bands) and high (sub-bands of the gamma band) frequency ranges, as well as the full EEG bandwidth (broadband).

2.4. Decoder models

In Dataset 1, amplitudes in all EEG channels at the current time point, as well as six lags prior, were utilized to infer the participants' current directional movement parameters (positions and velocities in both cartesian axes). The decoder consisted of Partial Least Squares (PLS) regression, followed by the subsequent application of an Unscented Kalman Filter (Martinez-Cagigal et al., 2020). In contrast, the initial version of our movement decoder used for Dataset 2 (recorded prior to Dataset 1) utilized a combination of PLS regression and a regular Kalman Filter, which proved to underestimate the amplitudes of the decoded kinematics (Mondini et al., 2020). Participants reported having to increase the range of motion of their dominant arm to compensate for the decrease in amplitude introduced by the decoder. This led to a large mismatch in the kinesthetic perception of movement and visual feedback during the fully EEG-controlled runs, even though the decreasing decoded amplitudes visually led to a decrease in the Euclidean error between target and feedback overall due to decreased peak-to-peak differences during instances of phase-shifts between target and decoded positions. In subsequent studies, Kobler and Martínez-Cagigal and colleagues (Kobler et al., 2020; Martinez-Cagigal et al., 2020) succeeded in eliminating this amplitude mismatch by including nonlinear non-directional movement parameters (distance, speed) in the PLS regression, exchanging the previously used Kalman Filter with an Unscented Kalman Filter. Dataset 1 (Pulferer et al., 2022) was finally recorded utilizing this extended approach and as such, the participants perceived the mismatch of target and feedback unaltered and strictly visually, in contrast to the kinesthetic perception mentioned for Dataset 2.

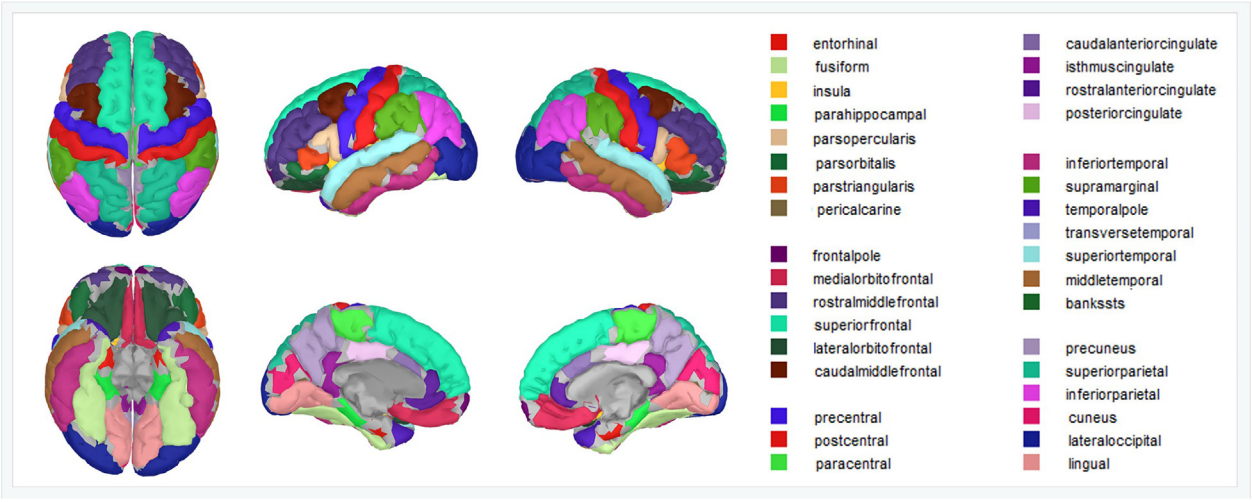

Fig. 2. Depiction of all 34 bilateral cortical regions of interest as defined within the Desikan-Killiany atlas.

2.5. Data analysis

2.5.1. Sensor space

We performed data analysis in all datasets using MATLAB and EEGLAB (Delorme and Makeig, 2004). To quantify the cognitive response to an increasingly erroneous feedback signal, we estimated the Euclidean error signal between target and feedback, i.e., between snake and feedback dot positions for Dataset 1 and the participant with SCI, and between snake and assistive robotic arm positions in Dataset 2 for each of the feedback conditions. The sinusoidal patterns of the depicted target trajectory (see Fig. 1A1–3, B1–4) translated to the feedback's kinematics as well. As such, we chose to locate local maxima of the Euclidean error signal and time-lock the EEG (preprocessed and bandpass filtered as described before) in epochs of [−1,3]s within these maxima (see Fig. 1A-B). The epochs obtained in this manner were then averaged within subjects for each condition.

2.5.2. Source space

Complementing the time series analysis in sensor space, we additionally investigated the origin of the measured EEG signals by back-projecting to source space via Brainstorm (version 17-May-2022, (Tadel et al., 2011)). As in previous studies (Mondini et al., 2020; Srisrisawang and Müller-Putz, 2022), we obtained head models for all participants and sessions using OpenMEEG (Gramfort et al., 2010). The ICBM152 boundary element model (BEM) (Kybic et al., 2006) was then co-registered to the individual electrode positions recorded prior to each measurement session (ELPOS, Zebris Medical GmbH, Germany). We adjusted the standard conductivity values in each of the three layers of the BEM, comprising cortex, skull, and scalp conductivity, to (1, 0.008, 1). Projection onto the template head model's surface alleviated deviations of the electrode positions from the standard BEM due to individual head geometries. To estimate the channel noise covariance matrix for generating forward and inverse solutions, resting state data of each session, preprocessed as described in Section 2.3, were used. For numerical stability, we regularized the noise covariance matrix by adding an identity matrix scaled to 10% of the largest eigenvalue. The use of sLORETA (Pascual-Marqui, 2002) provided an inverse solution via minimum norm imaging. We restrained the model by only considering dipoles with an orientation normal to the cortex, leading to solutions to the inverse problem featuring one source dipole in each of the 15,000 vertices. For subsequent analysis and statistical testing, the full cortical map with constrained dipole orientations was downsampled to the Desikan-Killiany atlas (Desikan et al., 2006), consisting of 68 regions of interest spanning the whole cortex (see Fig. 2). We specifically chose this atlas to obtain a fundamental understanding of the cortical activations elicited during error processing.

2.6. Estimation of directional connectivity

To establish how different cortical areas communicate during error processing, connectivity within the regarded time series was inferred according to Granger's and Wiener's concept of causality (Granger, 1969). Specifically, we can assume a causal connection between two time series if past information of one time series improves the prediction of the other time series. In this context, multivariate autoregressive (MVAR) models that describe the current state of each time series as a linear combination of its own as well as other time series' histories can find use. An MVAR model most generalized takes the form

$$\boldsymbol{y}(n) = \sum_{k=1}^{p} \boldsymbol{A}_k \boldsymbol{y}(n-k) + \boldsymbol{\varepsilon}(n) = \boldsymbol{A}\boldsymbol{\varphi}(n) + \boldsymbol{\varepsilon}(n), \tag{1}$$

where $\boldsymbol{y}(n) \in (\mathbb{R})^{M\times 1}$ is the multivariate time series at time point $n = 1\ldots N$ with N being the total number of samples and M the number of time series under consideration. Further, p describes the model order, $\boldsymbol{A}_k \in (\mathbb{R})^{M\times M}$ corresponds to the coefficient matrix for $k \in [1, p]$ $(\boldsymbol{A} = [\boldsymbol{A}_1 \ldots \boldsymbol{A}_p] \in (\mathbb{R})^{M\times Mp})$, $\boldsymbol{\varphi}(n) = [\boldsymbol{y}(n-1) \ldots \boldsymbol{y}(n-p)]^T \in (\mathbb{R})^{Mp\times 1}$ describes the regressor vector consisting of past lags from all time series and $\boldsymbol{\varepsilon}(n) \in (\mathbb{R})^{M\times 1}$ is zero-mean white noise, known also as innovation process vector. In matrix form, Eq. (1) can be written as $\boldsymbol{Y} = \boldsymbol{A}\boldsymbol{\Phi} + \boldsymbol{E}$, whereby $\boldsymbol{Y}$, $\boldsymbol{E} \in (\mathbb{R})^{M\times N}$ and the regressor matrix $\boldsymbol{\Phi} \in (\mathbb{R})^{Mp\times N}$. The coefficient matrix can be estimated using the Least Squares approach. Here, we opted to use the Arfit module which is based on a stepwise least squares algorithm for MVAR estimation (Schneider and Neumaier, 2001; Schlögl, 2006).

To capture generalized connectivity patterns, we fitted MVAR models on EEG data from all subjects. The EEG data, averaged within each subject, were concatenated generating a matrix of the form $\boldsymbol{Y} \in (\mathbb{R})^{M\times NS}$ where S is the number of subjects accounted for. The regressor matrix is now of dimensionality $\in (\mathbb{R})^{Mp\times NS}$. In the case of Dataset 1, we considered $M = 56$ time series comprising 55 EEG channels as well as the Euclidean error signal between target and feedback. The total number of subject averages per condition was $S = 30$ (i.e., 3 session averages from 10 subjects), and the considered epoch length was $N = 801$ time points. For Dataset 2, we fitted an MVAR model on 60 time series ($M = 60$), consisting of 59 EEG channels plus the Euclidean error signal from $S = 10$ subject averages per condition (i.e., 1 session average from 10 subjects), and the same number of time points as in Dataset 1. As each MVAR model critically depends on the model order p, the

optimum model order p_{opti} was selected using the Akaike Information Criterion (AIC) (Akaike, 1974). The AIC considers the fit of the model based on the residual errors ($\boldsymbol{\Sigma} = cov(\boldsymbol{Y} - \tilde{\boldsymbol{Y}})$, with $\tilde{\boldsymbol{Y}}$ the prediction of the model) and penalizes the total number of MVAR coefficients as $AIC(p) = N \cdot log(|\boldsymbol{\Sigma}|) + 2 \cdot M^2 p$. We selected the optimum model order as the knee of the function $AIC(p)$.

Aside from a time domain description of causality, oscillatory content within the data may be explored in the frequency domain (Saito and Harashima, 1981; Akaike, 1998; Baccala et al., 1998). As the lag operator transforms as $F\{\boldsymbol{Y}(n-k)\} = exp(-2\pi i k N f)\boldsymbol{Y}(f)$, with $\boldsymbol{Y}(f)$ the Fourier transform of $\boldsymbol{Y}(n)$, the MVAR model in the frequency domain may be expressed as: $\boldsymbol{Y}(f) = \boldsymbol{H}(f)\boldsymbol{E}(f)$, where $\boldsymbol{H}(f) = [\boldsymbol{I} - \sum_{k=0}^{p} \boldsymbol{A}_k exp(-2\pi i k N f)]^{-1}$ describes the transfer matrix. The entries of this transfer matrix $\boldsymbol{H}(f)$, derived from the coefficient matrices $\boldsymbol{A}_k$ in the time domain, can then be used to infer directional connectivity, known also as directed coherence (DC) (Baccala et al., 1998):

$$DC(f)_{td} = \frac{\sigma_d \; H(f)_{td}}{\sqrt{\sum_{m=1}^{M} \sigma_m^2 |H(f)_{tm}|^2}}, \tag{2}$$

with $\sigma_j^2, \; j = 1 \ldots M$ the diagonal entries of the diagonal covariance matrix $\boldsymbol{\Sigma} = diag(\sigma_1^2, \; \ldots \sigma_M^2)$, as estimated from the residuals of the MVAR model due to the lack of a priori knowledge of the innovation process covariance matrix. In detail, $\boldsymbol{DC}(f) \in (\mathbb{R})^{M \times M}$ of Eq. (2) corresponds to an asymmetric matrix, wherein each entry DC_{td} describes the direct and indirect power contributions of a driving signal d to a target signal t. To estimate the influence of the Euclidean error signal over all other (EEG) channels, we thus considered only the entries of the DC matrix corresponding to the error as a driving signal. For the estimation of the DC matrix, we utilized the eMVAR toolbox (Faes et al., 2013). As our data consisted of both multichannel EEG signals (μV) and the calculated Euclidean error signal between target and feedback (pixels / px) from different subjects, we standardized all signals prior to MVAR fitting to remove subject- and signal- specific scale dependencies. To evaluate statistical significance in each condition, $n = 50$ surrogate signals were generated (Faes et al., 2010; Kostoglou and Müller-Putz, 2021; Wimmer et al., 2022). In detail, we created artificial (surrogate) signals by transforming our datasets to the frequency domain, randomly shuffling their phases, and back-transforming to the time domain again. For each batch of back-projected surrogate signals, now lacking any causal relation, we then estimated an MVAR model of model order p_{opti} and calculated the corresponding DC matrix. As an estimator for the statistical threshold, we then used the 95th percentile of the 50 estimated DC values. Finally, all values below the threshold were set to zero, implying no significant causal contribution from these specific target-to-driver combinations.

3. Results

3.1. Dataset 1

In the following sections we present the grand average EEG signals for the slightly delayed feedback (correct), the slight error and the severe error conditions (grand average per condition) of Dataset 1. To investigate discrepancies between the perception of slightly delayed feedback versus erroneous feedback, we also evaluated pairwise differences between feedback conditions (grand average differences between conditions). We outline these differences in conditions, ranging from delayed feedback to severely erroneous conditions, both in sensor and source space.

3.1.1. Sensor space

3.1.1.1. Grand average per condition. As previously shown in (Pulferer and Müller-Putz, 2022), the discrepancy between target and feedback clearly modulated the grand average scalp potentials within the erroneous conditions featured in Dataset 1 (Fig. 3). While we also report periodic behavior above occipital regions in the Delayed Feedback condition (top line topographical maps), both Slight and Severe Error conditions (middle and bottom line topographical maps) displayed consistent scalp topographies coupled to the phase of the Euclidean error signal. Specifically, we observed a prominent phase-lock of fronto-central negative deflections to minima in the Euclidean error signal, while fronto-central positive deflections coincided with maxima in the Euclidean error signal.

3.1.1.2. Grand average differences between conditions. In line with previous research on the processing of discrete error stimuli, we subsequently analyzed all pairwise differences that arose from the three feedback conditions Delayed Feedback, Slight Error, and Severe Error (cf. Fig. 1A).

Topographical maps displaying these three pairwise differences, i.e., Slight Error-Delayed Feedback, Severe Error-Delayed Feedback, and Severe-Slight Error, are shown in Fig. 4A, from top to bottom. We report a strong fronto-central negativity around the first minimum of the Euclidean error signal at t=−1s, followed by a central positivity coinciding with the maximum of the Euclidean error signal at $t = 0$s. This phase-locked behavior of the difference signals persisted throughout the epoch length and arose again with centro-parietal negativities at t = [0.75, 2.25]s, as well as a weak but distinct centro-parietal positivity around $t = 1.5$s. A paired permutation t-test on all session averages ($n = 30$) between the condition pairs (3) in all time points (801), channels (55) and frequency bands of interest (12) revealed significant differences between delayed feedback and both erroneous feedback conditions (Fig. 4A, top and middle line topographical maps; significant differences marked as black '+') throughout the whole epoch length in the delta, low and broad frequency bands. We corrected for multiple comparisons ($N = 3 \times 55 \times 801 \times 12$ tests) using the False Discovery Rate (FDR) (Benjamini and Hochberg, 1995) at a significance level of 0.05. In contrast, we observed minimal significant differences between both erroneous feedback conditions (Fig. 4A, bottom line topographical maps), with the most prominent disparity around $t = 0.75$s. Results of Fig. 4 depict findings in the delta band only; the findings for the low and broad frequency bands are shown in Fig.S2A and Fig.S3A, respectively (supplementary material). Additional information on mean and total number of epochs investigated for each feedback condition within Dataset 1 are listed in Table 3.

3.1.2. Source space

In addition to the time series analysis in sensor space, we projected the average signals per condition of each participant to source space as well. To gain a deeper understanding of the functionally involved cortical areas, we downsampled the full cortical maps to the Desikan-Killiany atlas (Fig. 2). For all conditions, time points, and frequency bands of interest (see Table 2), the mean of all voxels in each of the 68 regions of interest was calculated. As in the sensor space analysis, pairwise differences between the signals of different conditions were calculated. We employed a permutation paired t- test to compare the conditions, utilizing FDR correction ($N = 3 \times 68 \times 801 \times 12$ tests) at a significance level of 0.05. Statistical analysis revealed significant differences between delayed feedback and both erroneous conditions of Dataset 1 in the delta, low and broad frequency bands. The results for all three comparisons in Dataset 1 in the delta frequency band are presented in Fig. 4B (Slight Error-Delayed Feedback, Severe Error-Delayed Feedback, and Severe-Slight Error, left to right). The supplementary material provides results pertaining to the low and broad frequency bands (Fig.S2–3B). The vertical black line at $t = 0$s corresponds to the local maximum of the Euclidean error signal. Black outlined rectangles mark significantly differing periods arising in each scout, whereas black outlined diamonds at the right edge of each plot mark scouts exhibiting at least one such period of significance throughout the epoch for a better overview. For the comparison of delayed feedback versus erroneous conditions (left and middle panels), we detected significant differences

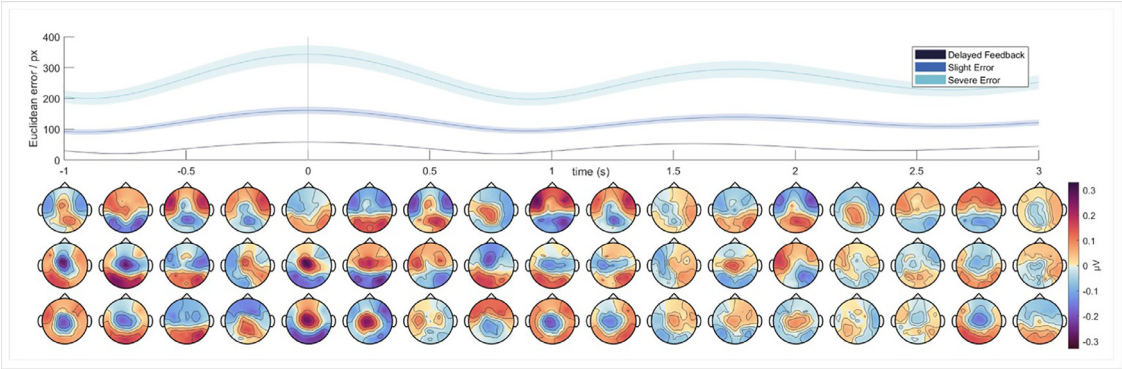

Fig. 3. Dataset 1. Topographical maps of the grand average electroencephalographic signals, time-locked at $t = 0$s to local maxima of the Euclidean error signal (time series, top) between target (snake) and feedback (feedback dot), for Delayed Feedback, Slight Error, and Severe Error conditions (topographical maps, top down). All depicted results correspond to findings in the delta band.

Table 3
Total number of epochs and mean number of epochs per participant with standard deviation (STD) for the three feedback conditions in Dataset 1.

Dataset 1	Delayed feedback	Slight error	Severe error
Total Nr. of Epochs	10,387 (avg.: 7.2 epochs/trial)	6818 (avg.: 6.3 epochs/trial)	5558 (avg.: 5.1 epochs/trial)
Mean Nr. of Epochs (STD)	346 (30)	227 (28)	205 (77)

throughout the epoch length in most scouts of the atlas. To capture the order of engagement of distinct cortical regions, we sorted the scouts based on the time of appearance of the first maximum in the amplitude of each scout. This revealed a wave-like pattern propagating through the atlas as single scouts engaged sequentially in response to the Euclidean error signal. Remarkably, the order of engagement of the single scouts was approximately the same for both condition differences (see Fig. 5). Furthermore, significant differences in both comparisons largely coincided, suggesting specific regions of interest as the main contributors to erroneous feedback processing within the brain. In detail, we report significant differences between the delayed feedback and both erroneous conditions bilaterally in the parahippocampal and middle temporal gyri, posterior cingulate cortex, insula, and the banks of the superior temporal sulcus (Fig. 4B, 'Slight Error-Delayed Feedback', 'Severe Error-Delayed Feedback'). Further, we observed significant differences in the contralateral supramarginal and rostral middle frontal gyri, as well as the caudal anterior cingulate and entorhinal cortices. Ipsilaterally, both inferior and transverse temporal, as well as caudal middle frontal gyri must be mentioned, along with parietal areas spanning inferior parietal lobule and precuneus. In contrast to these findings, no outstanding differences can be reported between both erroneous conditions (see Fig. 4B, right panel).

In addition to the analysis regarding the regions of interest, we further analyzed the differences between conditions across the whole cortex. The resulting grand average full cortical maps for all pairwise differences in Dataset 1 are shown in Fig. 4C (Slight Error-Delayed Feedback, Severe Error-Delayed Feedback, and Severe-Slight Error, top down). As employed in (Tadel et al., 2019), we smoothened the source maps strictly containing dipoles normal to the cortex to alleviate individual influences on the grand average results. The smoothing was implemented by (Worsley et al., 2009) based on a Gaussian kernel scaled to the dimensions of the cortical mesh (full width half maximum = 10mm). Consistent with the findings in sensor space, modulations in the difference between delayed feedback and erroneous signals arose in the cortex as well. Differences between delayed feedback and erroneous conditions on the contralateral frontal cortex, spanning the area from the precentral gyrus to the caudal middle and superior frontal gyrus, appeared phase-locked to the Euclidean error signal in a similar fashion as observed in sensor space. In addition, we report modulations in the bilateral postcentral gyri and the parietal lobules throughout the whole epoch length. Regarding both erroneous conditions, amplitude differences appeared strongly attenuated, akin to the findings observed in sensor space (Fig. 4C, bottom line cortical maps).

3.2. Dataset 2

As for Dataset 1, we present the grand average EEG signals of Dataset 2 for the slightly delayed feedback (correct), minimal, moderate and severe error conditions in the following sections. To analyze differences between the perception of delayed feedback versus erroneous feedback, we again evaluated the differences between pairs of conditions both in sensor and in source space.

3.2.1. Sensor space

3.2.1.1. Grand average per condition. As with Dataset 1, we observed increasing modulations in the grand average EEG signals with increasing discrepancy between target and feedback in sensor space (Fig. 6). In contrast to the grand average signals in the Delayed Feedback condition (1st row topographical maps), we observed similar patterns in the scalp potentials for the Minimal, Moderate and Severe Error conditions (2nd to 4th row topographical maps, respectively). Similar to the findings in Dataset 1, a centro-parietal negativity arose shortly after minima in the Euclidean error signal, followed by a fronto-central positive deflection coinciding with maxima in the Euclidean error signal.

3.2.1.2. Grand average differences between conditions. As for Dataset 1, we subsequently analyzed all possible pairwise differences between the conditions Delayed Feedback, Minimal Error, Moderate Error and Severe Error (cf. Fig. 1B), leading to six comparisons. Topographical maps of three of the six pairwise differences (Severe-Minimal Error, Severe Error-Delayed Feedback, and Minimal Error-Delayed Feedback) are presented in Fig. 7A, from top to bottom. The remaining difference plots can be found in Fig.S4 (supplementary material).

Similar to the findings for Dataset 1, the difference patterns in Dataset 2 for Delayed Feedback/Minimal Error in comparison with the Severe Error condition (Fig. 7A, top and middle line topographical maps) appeared in phase with the modulations of the Euclidean error signal between target and feedback, while differences between Delayed Feedback and Minimal Error (Fig. 7A, bottom line topographical maps)

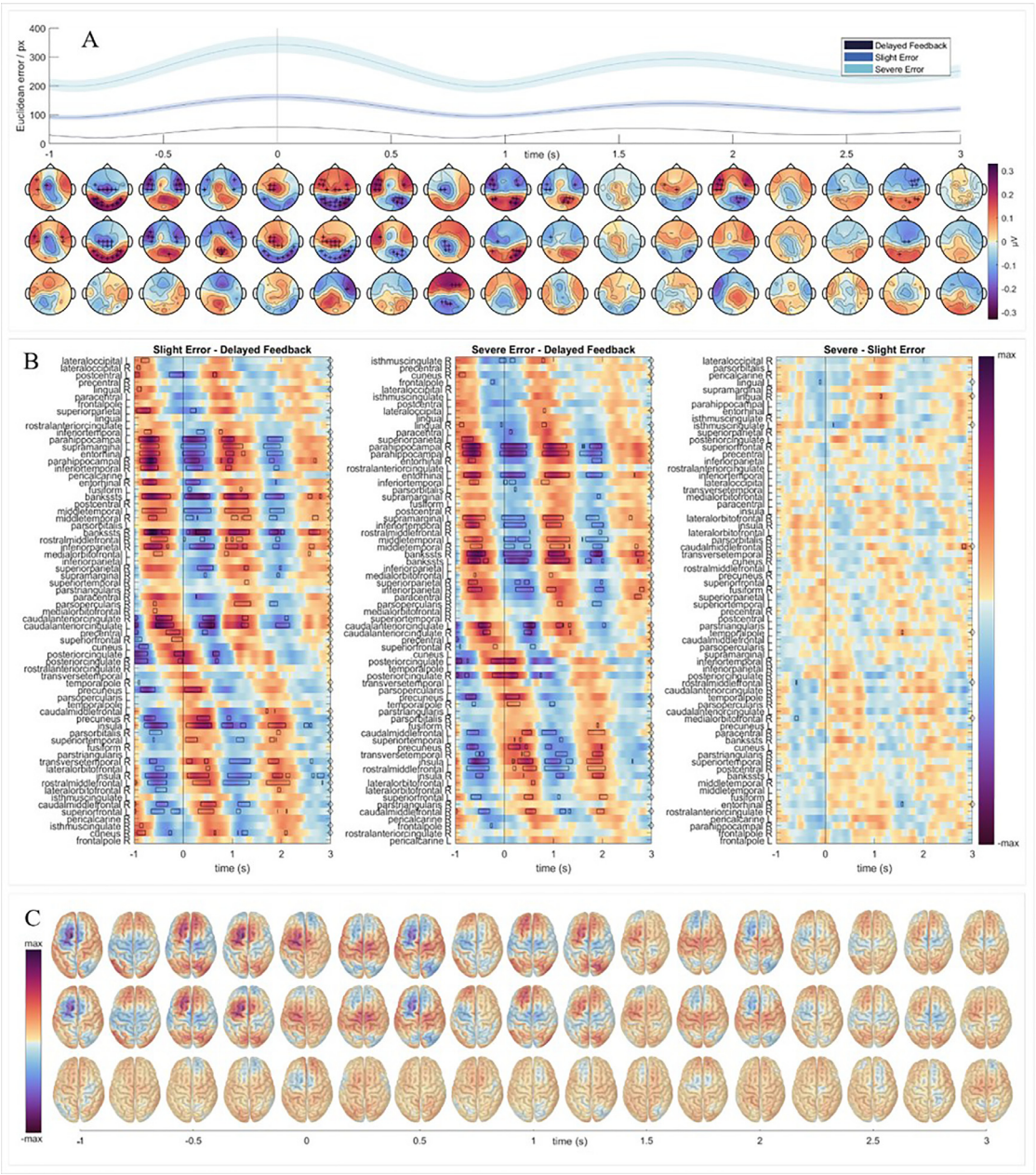

Fig. 4. Dataset 1. A (top) Grand average Euclidean error signal between target (snake) and feedback (feedback dot) for the three feedback conditions Delayed Feedback, Slight Error, and Severe Error. **(bottom)** Grand average difference patterns in the EEG signals, time-locked to local maxima of the Euclidean error signal ($t = 0$ms) for Slight Error-Delayed Feedback, Severe Error-Delayed Feedback, and Severe-Slight Error conditions (topographical maps, top down). Channels displaying significant differences are marked with a black '+'. **B** Grand average difference patterns in the cortical regions of interest (scouts) for Slight Error-Delayed Feedback, Severe Error-Delayed Feedback, and Severe-Slight Error conditions (left to right). Periods of significant difference are marked with black outlined rectangles, scouts exhibiting at least one period of significance are marked with a black outlined diamond to the right. **C** Grand average full cortical difference patterns for Slight Error-Delayed Feedback, Severe Error-Delayed Feedback, and Severe-Slight Error conditions (top down). All depicted results correspond to findings in the delta frequency band.

showed slight attenuation in comparison. Further, we report a centro-parietal negativity coinciding with local minima of the Euclidean error signal for Dataset 2 (cf. Fig. 7A, $t = [-0.5, 1, 2.5]$s), along with a fronto-central positivity around local maxima (cf. $t = [0.25, 2]$s), as observed for Dataset 1. However, the difference patterns between Delayed Feedback/Minimal Error and Severe Error conditions exhibited a delay of around 0.25s compared to the results observed in Dataset 1.

Regarding the grand average signals, a permutation paired t-test was employed. However, with six pairwise comparisons, along with a larger number of EEG channels (59), the number of tests demanding FDR correction at a significance level of 0.05 more than doubled ($N = 6 \times 59 \times 801 \times 12$ tests). Unlike the results observed in Dataset 1, statistical testing revealed no significant difference in any of the six pairwise comparisons or 12 frequency bands of interest. Additional information on mean and total number of epochs investigated for each feedback condition within Dataset 2 are listed in Table 4.

As only the Delayed Feedback and Severe Error conditions were shared in both datasets, a direct comparison was limited to the Severe Error-Delayed Feedback difference signal. This comparison revealed coinciding difference patterns in the scalp potentials (see Fig. 4A and

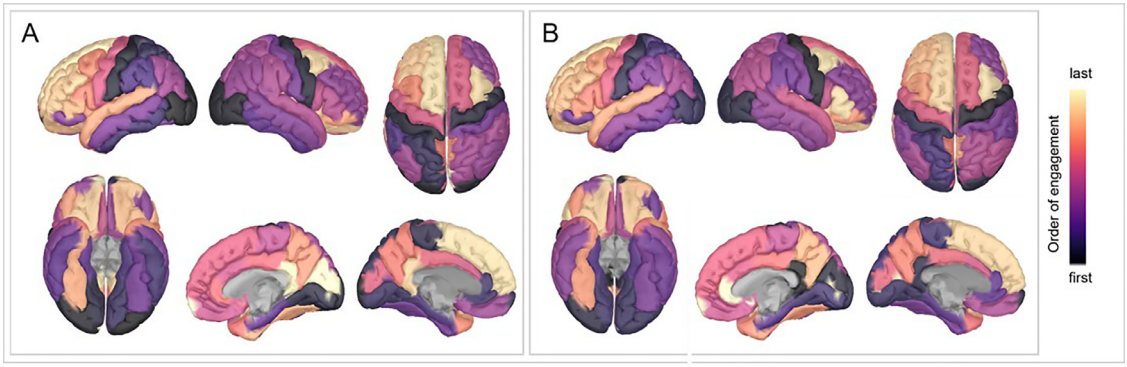

Fig. 5. Dataset 1. Order of engagement (from first to last) of each scout in the **A** Slight Error-Delayed Feedback and **B** Severe Error-Delayed Feedback condition differences.

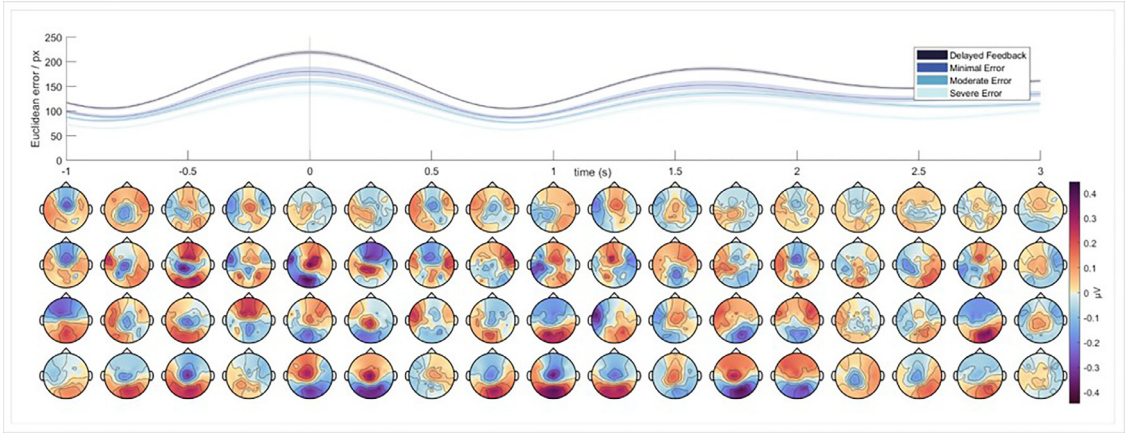

Fig. 6. Dataset 2. Topographical maps of the grand average electroencephalographic signals, time-locked at $t = 0$s to local maxima of the Euclidean error signal (time series, top) between target (snake) and feedback (assistive robotic arm), for Delayed Feedback, Minimal Error, Moderate Error and Severe Error conditions (topographical maps, top down). All depicted results correspond to findings in the delta band.

Table 4
Total number of epochs and mean number of epochs per participant with standard deviation (STD) for the four feedback conditions in Dataset 2.

Dataset 2	Delayed Feedback	Minimal Error	Moderate Error	Severe Error
Total Nr. of Epochs	4093 (avg.: 6.8 epochs/trial)	1975 (avg.: 8.2 epochs/trial)	2333 (avg.: 9.7 epochs/trial)	2131 (avg.: 8.9 epochs/trial)
Mean Nr. of Epochs (STD)	409 (74)	198 (49)	233 (58)	213 (46)

Fig. 7A, middle line topographical maps). Furthermore, the grand average feedback conditions showed similar scalp potentials in the Severe Error condition for both datasets (see Figs. 3 and 6; bottom line topographical maps).

3.2.2. Source space

As for Dataset 1, we projected the average signals per condition of each participant to source space as well for Dataset 2, and downsampled the full cortical maps to the Desikan-Killiany atlas (Fig. 2). The grand average results on the scouts in Dataset 2 for three of the six pairwise comparisons (Severe-Minimal Error, Severe Error-Delayed Feedback, and Minimal Error-Delayed Feedback) are shown in Fig. 7B; remaining difference plots can be found in Fig.S4 (supplementary material). The vertical black line at $t = 0$s corresponds to the local maximum of the Euclidean error signal. Contrary to the results on Dataset 1, statistical analysis ($N = 6 \times 68 \times 801 \times 12$ tests) revealed no significant differences between any pairs of conditions in any frequency band of interest. However, sorting the scouts according to the first appearance of a local maximum in each scout again, we observed qualitatively similar difference patterns across the atlas as in Dataset 1 for the Severe Error-Delayed Feedback difference (Fig. 7B, middle panel). In contrast to Dataset 1, the arising patterns were less prominent for all differences in conditions, possibly due to the smaller number of participants. Nonetheless, error-induced modulations of the single scout signals remained visible, suggesting a common cognitive process that arises with error perception and processing in both investigated datasets.

An analysis of the full cortical maps of the grand average differences in Dataset 2 revealed qualitatively similar, though overall more erratic source patterns than observed for Dataset 1 (Fig. 7C). For lack of space, we again only show the difference projections in formerly mentioned condition pairs; the remaining comparisons can be found in Fig.S4 (supplementary material). Focusing on the difference between the only shared pair of conditions in Dataset 1 and Dataset 2 (see Fig. 4C and Fig. 7C, middle line cortical maps), i.e., the Severe Error-Delayed Feedback difference, comparable patterns were observed. Interestingly however, the results in Dataset 2 appeared slightly less lateralized, with the largest differences being centered around the sagittal midline in the bilateral superior frontal and precentral gyri, as well as the parietal lobules.

3.3. Spinal cord injured participant

Following the time series analyses on Datasets 1 and 2, we investigated pre-recorded data of a participant with SCI to analyze common

Fig. 7. Dataset 2. A (top) Grand average Euclidean error signal between target (snake) and feedback (assistive robotic arm) for the four feedback conditions Delayed Feedback, Minimal Error, Moderate Error, and Severe Error. **(bottom)** Grand average difference patterns in EEG signals, time-locked to local maxima of the Euclidean error signal ($t = 0$ms) for Severe-Minimal Error, Severe Error-Delayed Feedback and Minimal Error-Delayed Feedback feedback conditions (topographical maps, top down). **B** Grand average difference in the scout signals for Severe-Minimal Error, Severe Error-Delayed Feedback and Minimal Error-Delayed Feedback conditions (left to right). **C** Grand average full cortical difference maps for Severe-Minimal Error, Severe Error-Delayed Feedback, and Minimal Error-Delayed Feedback conditions (top down). All depicted results correspond to findings in the delta frequency band.

cognitive processes during error processing between participants experiencing no versus a complete loss of motor output. Collective results in the dataset recorded from the participant with SCI, both in sensor and in source space, are presented in Fig. 8. An analysis of the pairwise differences in sensor space between the three delivered feedback conditions (Fig. 8A, topographical maps; Slight/Severe Error-Delayed Feedback, Severe-Slight Error, top down) revealed comparable difference patterns to those observed within Datasets 1 and 2. Although here the findings corresponded to a single participant, the difference patterns between delayed feedback and erroneous conditions (Fig. 8A, top and middle line topographical maps) exhibited matching characteristics with the ones obtained from the 30 sessions in the able-bodied participants comprising Dataset 1. Again, we report fronto-central positivities at, and even shortly before, local error maxima, followed by centro-parietal negativities corresponding to local minima of the Euclidean error signal. Further comparisons (see Fig.S5, supplementary material) revealed that the observed modulations appeared in both erroneous conditions as well in the participant with SCI, while no modulation was seen in the delayed feedback condition. However, the observed Severe-Slight Error differences in the SCI participant remained largely undamped (Fig. 8A, bottom line topographical maps), in contrast to the dissipating difference signals observed in Dataset 1. Additional information on the number of epochs investigated for each feedback condition in the participant with SCI are listed in Table 5.

Regarding source space projection, the difference maps in the participant with SCI appeared more obscure both for the regions of interest de-

Fig. 8. Participant with spinal cord injury. A (top) Grand average Euclidean error signal between target (snake) and feedback (feedback dot) for the three conditions Delayed Feedback, Slight Error, and Severe Error. **(bottom)** Grand average difference in electroencephalographic signals, time-locked to local maxima of the Euclidean error signal ($t = 0$ms) for Slight Error-Delayed Feedback, Severe Error-Delayed Feedback, and Severe-Slight Error conditions (topographical maps, top down). **B** Grand average difference in the scout signals for Slight Error-Delayed Feedback, Severe Error-Delayed Feedback, and Severe-Slight Error conditions (left to right). **C** Grand average full cortical difference maps for Slight Error-Delayed Feedback, Severe Error-Delayed Feedback, and Severe-Slight Error conditions (top down). All depicted results correspond to findings in the delta frequency band.

Table 5
Total number of epochs for the three feedback conditions in the participant with SCI.

Participant with SCI	Delayed feedback	Slight error	Severe error
Total Nr. of Epochs	290 (avg.: 6.0 epochs/trial)	138 (avg.: 5.8 epochs/trial)	156 (avg.: 6.5 epochs/trial)

fined in the Desikan-Killiany atlas (Fig. 8B), as well as for the full cortical maps (Fig. 8C). The resulting difference signals on the regions of interest maintained high amplitudes in all three comparisons (Fig. 8B), even in the comparison between both erroneous conditions (right panel). However, the same modulation as seen already for Datasets 1 and 2 arose in the difference signals of delayed feedback and both erroneous signals (left and middle panel). Similar conclusions could be drawn regarding the full cortical maps. Considering the differences between delayed feedback and both erroneous conditions ('Slight Error-Delayed Feedback', 'Severe Error-Delayed Feedback'; Fig. 8C, top and middle line cortical maps), we observed central and centro-parietal positivities around $t = [-0.25, 1.25]$s, roughly coinciding with the local maxima of the Eu-

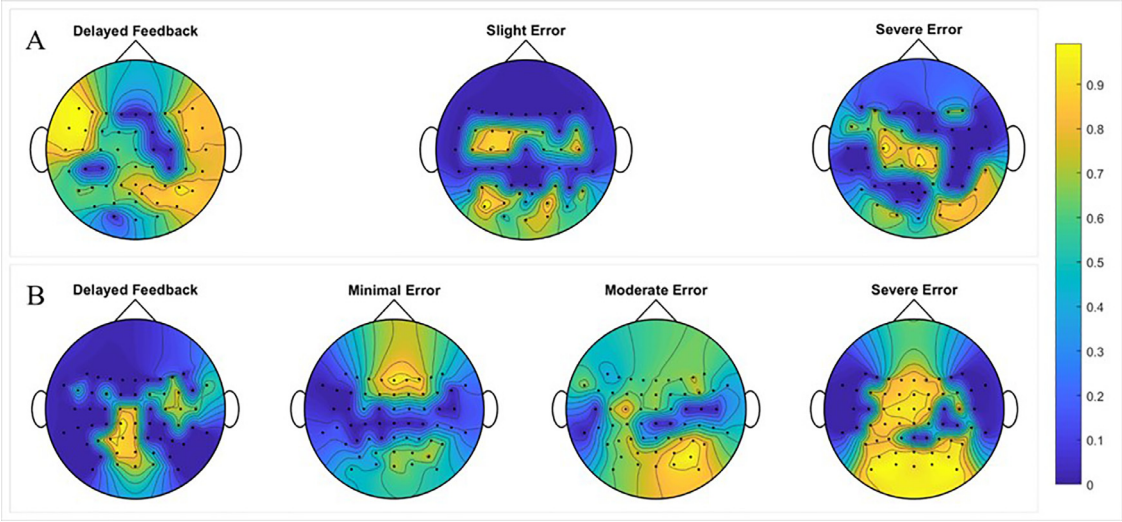

Fig. 9. Directed Coherence from the Euclidean error signal (driving time series) to the EEG channels (target time-series) in **A** Dataset 1 for Delayed Feedback, Slight, and Severe Error conditions (left to right), and **B** Dataset 2 for Delayed Feedback, Minimal, Moderate, and Severe Error conditions (left to right). For both datasets, increasing engagement of central and occipital areas from delayed feedback to severely erroneous feedback conditions can be observed. The depicted results correspond to findings in the delta band. Each map was normalized concerning its maximum DC value to ensure comparability between conditions and datasets.

clidean error signal. Additionally, we report slight parietal negativities around $t = [0.5, 2]$s, approximately at or slightly before local minima of the Euclidean error signal. However, compared with the grand average signals of the 30 able-bodied participants comprising Dataset 1, the overall difference patterns on the cortex naturally appeared less distinct and erratic.

3.4. Directional connectivity analysis

Investigating a range of different model orders ($p \in [1,\ 50]$), the optimum model order for Dataset 1 was found to be $p_{opti} = 27$, and the optimum order for Dataset 2 was identified as $p_{opti} = 14$. For both datasets, a time window of [−2,2]s within each local Euclidean error signal maximum was selected. This symmetric time window was chosen to minimize averaging effects which dilute the signals in time points of larger temporal distance to the time-locked first maximum ($t = 0$ms) .[1]

We only considered DC values from the Euclidean error signal to all investigated EEG channels in the delta band. The estimated DC for Datasets 1 and 2 is presented in the form of topographical maps in Fig. 9A and 9B, respectively. The findings revealed increasing information outflow from the error signal towards contralateral central as well as bilateral occipital areas with increasing erroneous feedback for both datasets. Specifically, these areas spanned regions above the contralateral primary motor, as well as the visual cortices, which increasingly engaged with progressively erroneous feedback. Noticeably, however, the DC patterns in the Delayed Feedback condition differed considerably between datasets. During the attempted movement employed in Dataset 1, where feedback was exclusively delivered on-screen, we observed high information outflow bilaterally towards the scalp regions above the inferior frontal and caudal middle frontal gyri. Similarly, high DC values were shown ipsilaterally for areas covering the superior and inferior parietal lobules. In contrast, limited information outflow arose in mentioned areas for Dataset 2, with high contributions in the contralateral parietal regions overlapping the cortical areas containing both cuneus and precuneus.

[1] In prior analyses, the asymmetric window of [−1,3]s was chosen to investigate both the characteristics immediately prior to, and the periodicity arising with additional local extrema after each local Euclidean error signal maximum (t = 0ms).

4. Discussion

Within our analysis of two prerecorded datasets investigating continuous target tracking combined with increasingly erroneous feedback, we present three major results.

First, a neural correlate to continuous error processing not only exists but can furthermore be distinguished without previously defined error onsets. We succeeded in meaningfully time-locking the EEG signals to local maxima of the Euclidean error signal between target and feedback, revealing strong error-driven modulations in delta brain activity within all erroneous conditions. Connectivity analysis revealed an emerging centro-occipital network of error processing with increasingly erroneous feedback, suggesting an increase in both visual perception of the mismatch, and the focus on corrective motor output, ascribed to visual and motor cortices, respectively.

Second, the periodic target-feedback mismatch promotes a consistent cortical response. Source space analysis revealed a consistent order of engagement of different cerebral regions during continuous error processing across different severity levels of the perceived error. And third, a connection between the ERN/Pe and different cognitive components of error processing might tentatively be suggested. The continuous characteristics of the target-feedback mismatch employed in this study allowed to match source signals with the driving error signal at any point in time within the regarded epoch, relating cortical regions with specific time frames in error processing, which has, to our knowledge, not been investigated in this form before.

4.1. A correlate to continuous error processing

An in-depth analysis of two different datasets, comprising overall 40 sessions of data in 20 able-bodied participants, revealed strong modulations in both scalp potentials and estimated dipole sources with the Euclidean error signal between target and feedback. We report a periodic occurrence of centro-parietal negativities in the difference signals between delayed feedback and erroneous conditions coinciding with local minima in the Euclidean error signal, followed by fronto-central positivities around local maxima. Analyzing the grand average feedback conditions, these differences trace back to the erroneous conditions (Figs. 3 and 6). Furthermore, statistical analysis revealed a significant discrepancy between delayed feedback and erroneous conditions in the delta,

low and broad frequency band for the larger dataset (Dataset 1), both in the EEG sensor space and in the brain regions comprising the Desikan-Killiany atlas. As discussed in the original work (Mondini et al., 2020; Pulferer et al., 2022), the snake kinematics were sampled from pink noise, bandpass filtered between 0.2 and 0.4 Hz. We hypothesize that the specific importance of the delta band in the current work was inherited from the low-frequency movement of the depicted target. In contrast to the observed differences between slightly delayed and erroneous feedback conditions, marginally significant differences arose between both erroneous conditions. Taken together, these findings suggest that the observed modulations indeed reflect a cognitive response to the mismatch between target and feedback. Regarding Dataset 2, no significant differences arose. This lack of significance might tentatively be linked to the smaller number of only 10 sessions in Dataset 2 in comparison to the 30 sessions recorded within Dataset 1. However, we did not conduct a power analysis to gage the necessary number of sessions for the current work, as both datasets initially aimed to answer different research questions and literature advises against post-hoc analyses of this kind (Goodman and Berlin, 1994; Althouse, 2021).

Interestingly, we observed remarkable similarities between the established physiology of both ERN and Pe, and the centro-parietal negativity and consecutive fronto-central positivity measured in our data. We report clear and consistent cortical modulations resembling ERN and Pe during the exposure to a continuous error signal of varying severity despite the continuous exposure to an erroneous signal. However, additional analysis of Dataset 1 indeed showed declining amplitudes in the difference signals from session 1 to session 3 (see Fig. S6–8, supplementary material), which may be explained several fold. In line with the conflict-monitoring theory, decreasing interest or even decreasing perceived importance of the mismatch between target and feedback might have caused reduced perception of conflict during later sessions (Yeung et al., 2004). Indeed, each session depicted the exact same conditions of increasingly erroneous feedback, which arguably would lead to a loss of engagement and perceived urgency when faced with yet another deviation from the intended target state. Alternatively, reduced amplitudes with increasing session number might suggest a learning effect according to reinforcement-learning theory (Holroyd and Coles, 2002). In particular, the diminishing especially of the ERN-like scalp potentials coinciding with minima in the Euclidean error signal could be evidence of the proposed - yet unproven (Nieuwenhuis et al., 2002) - reduction of a feedback ERN with the acquisition of an internal input-output mapping. In particular, for the chosen objective of continuous movement decoding from the ongoing EEG the participants necessarily relied on a feedback dot portraying the current EEG-decoded positions on screen. As such, the feedback remained necessary for informing the participants of the current performance throughout the sessions, implying that the ERN-like potential corresponded strictly to a feedback ERN, which would strengthen the assumptions on learning raised by Holroyd and Coles (Holroyd and Coles, 2002). However, the same argument suggests that there was no skill set to acquire to begin with according to the proposed connection between feedback and response ERN. The consistent correlations between target and decoded positions across sessions reported in the original work substantiate this objection (Pulferer et al., 2022). Among all of the mentioned considerations regarding decreasing amplitudes across sessions, the conflict-monitoring theory appears to provide more powerful evidence.

Most interestingly, we observed coinciding results for Datasets 1 and 2. As stated, the movement decoding approach employed in Dataset 2 (Partial Least Squares Regression + Kalman Filter) introduced an amplitude mismatch between actual and decoded kinematics. We hypothesize that the reduced amplitudes of the decoded signals (feedback) finally lead to quantitatively decreasing Euclidean error between target and feedback, an effect which progressively surfaced as the amount of EEG-decoded positional information increased over the feedback conditions (0%, 50% and 100% for Dataset 1; 0%, 33%, 66% and 100% for Dataset 2). As discussed in the initial study (Mondini et al., 2020), the kinesthetic perception of increasingly erroneous feedback in Dataset 2 persisted nonetheless, as participants reported the need to increase their self-motion over the conditions to achieve comparable amplitudes. Thus, increasing error perception took place in the form of kinesthetic rather than visual feedback in Dataset 2. Nonetheless, the results coincided with findings in Dataset 1, where error perception occurred strictly via visual feedback. In addition, apart from the delay observed in Dataset 2 compared to Dataset 1, which likely represented the inertia of the assistive robotic arm employed (Fig. 1B), we observed similar difference patterns in both attempted and executed movement tasks. Taken together, these findings promote the robustness of this continuous correlate regarding the type of stimulus and error modality, which is in agreement with the results presented by Milter and colleagues (Miltner et al., 1997; Holroyd and Coles, 2002) on discrete error stimuli. Overall, these observations further suggest a direct connection between the observed ERN- and Pe-like scalp potentials and the actual ERN and Pe reported in context of discrete error stimuli.

Apart from these findings, the order of appearance of the ERN-like and Pe-like potentials might raise additional questions. Considering the time-locked behavior of the signals, the observed potentials seem to appear in a reversed order – Pe before ERN – compared to the known sequence reported in literature. However, due to the sinusoidal nature of the driving erroneous feedback signal, it appears problematic to mark a clear starting point to the process. Considering this, we argue that, starting from the initial deviation from the target, i.e., the minima in the erroneous feedback signal, the sequence of the reported potentials (ERN before Pe) actually aligns with previous research concerning discrete error stimuli.

Investigating the influence of the continuous error on the brain signals, connectivity analysis revealed engagement of one consistent centro-occipital network with an increasing mismatch between feedback and target (Fig. 9A-B, ‘Severe Error’). We observed stronger engagement of the contralateral central regions for Dataset 2, likely explained by higher-level motor activity during executed movement compared to the attempted movement task. Notably, however, clear differences could be detected between both datasets during the delayed feedback condition, both in the connectivity results (Fig. 9A-B, ‘Delayed Feedback’) and the EEG signals (Figs. 3 and 6, top line topographical maps, respectively), especially in the bilateral inferior frontal gyri. Previous reports linked these regions to inhibitory motor control (Swick et al., 2008; Hampshire et al., 2010), which matches the requirement of attempting, but not executing, movement as employed in Dataset 1. These findings suggest that inhibition of motor responses progressively loses importance when the participants are faced with an increasing mismatch between target and feedback.

Regarding the participant with SCI, we could not detect significant differences between conditions. However, the observed difference signals arose not only for able-bodied participants but for the participant with SCI as well. This appeared in line with previous works on the processing of discrete error stimuli, which reported the feasibility of measuring the ERN and Pe from participants with SCI (Keyl et al., 2018; Lopes-Dias et al., 2021) and suggests that the reported correlate for continuous error processing can play a role in BCI applications targeting actual end users. Although the results showed slightly erratic patterns in source space, as expected from single-participant results (Fig. 8B-C), the scalp potentials in the participant with SCI exhibited similar characteristics to those obtained from able-bodied participants (Figs. 4 and 7).

Altogether, our results promote that a neural correlate much akin to the ERN and Pe reported for discrete error stimuli emerges within continuous error processing.

4.2. Periodic feedback-target mismatch promotes periodic cortical response

Our results reveal strong EEG modulations by the Euclidean error signal between target and feedback. We observed significant differences

between delayed feedback and erroneous conditions in most scouts (Desikan et al., 2006), paired with minimal difference between both erroneous conditions, for Dataset 1 (Fig. 4B). This phase-locked behavior, though not significant (possibly due to the lower number of participants), emerged in Dataset 2 and the participant with SCI as well (Fig. 7B and Fig. 8B). Further analysis of the scouts exhibiting numerous periods of significant difference revealed bilateral engagement of the parahippocampal cortex (PHC) and middle temporal gyrus (MTG), posterior cingulate cortex (PCC), insula (IN), and the banks of the superior temporal sulcus (BanksSTS). Statistical testing revealed significance contralaterally in the supramarginal (SMG) and rostral middle frontal gyri (RMF), caudal anterior cingulate (cACC) and entorhinal (EC) cortices, and ipsilaterally in inferior (IT) and transverse (TT) temporal, caudal middle frontal (CMF) gyri, inferior parietal lobule (IPL) and precuneus (PCun). Comparing these regions and their respective time points of maximum amplitude with the corresponding Euclidean error signal, interesting insights emerge.

Remarkably, as the Euclidean error signal starts to increase (around t=−750 ms), we first observe maximum amplitude in the SMG and PHC, regions previously linked to rapid action reprogramming (Hartwigsen et al., 2012) and scene perception (Epstein and Kanwisher, 1998), both of which undoubtedly come in demand as target and feedback begin to deviate. In addition, the EC and medial temporal regions engage, which previously demonstrated a connection to motor learning and error detection in both humans and macaques (Hargreaves et al., 2012; Ku et al., 2021). Shortly afterwards, the BanksSTS, MTG and RMF activate, regions previously linked to the observation of reaching-to-grasp movement performed by an external agent (Kilintari et al., 2014), as well as during the observation of errors of commission in human participants (Laurens et al., 2003). Subsequently, cingulate regions (cACC, PCC) engage shortly prior to and coinciding with the maxima in the Euclidean error signal, areas which demonstrated importance during error and response detection in humans (Ursu et al., 2009) and in translating decision outcomes into higher-level strategies in macaque studies (Pearson et al., 2009), respectively. At a decreasing Euclidean error signal, we observe maximum amplitude in PCun, an area previously linked to shifting attention between different visual inputs as well (Wenderoth et al., 2005). In a final stage, IN and medial frontal regions engage. These areas are linked to error awareness (Klein et al., 2007; Hester et al., 2009) and response inhibition (Li et al., 2006) and presumably activate as the effort of correcting the erroneous response diminishes with decreasing deviation from the target. Interestingly, this sequence of engagement remained consistent over both erroneous conditions in Dataset 1 (Fig. 5) and reappeared with recurring Euclidean error signal modulations. Overall, these findings promote the periodicity of cognitive processes in the presence of periodic feedback-target mismatch, and - to our knowledge, for the first time - allow the identification of active brain regions at distinct stages of error processing.

4.3. The ERN, the Pe, performance monitoring, and corrective behavior

If we divide error processing into subcomponents of performance monitoring, error perception, error evaluation, and corrective behavior, we identify contributions of distinct cortical regions discussed before. The PHC, tasked with scene perception (Epstein and Kanwisher, 1998), as well as the BanksSTS and MTG connected to observation of reach-and-grasp movement (Kilintari et al., 2014) and action recognition and understanding (Herrington et al., 2011), offer all prerequisites for performance monitoring. In particular, the superior temporal sulcus reportedly engages during visual target stimulus processing (Pail et al., 2016), suggesting considerable importance within the employed paradigms. In a similar fashion, the RMF, MTG, and IN, related to the observation of error commission and error awareness, might pose as candidates for error perception (Laurens et al., 2003; Hester et al., 2009), while EC and cACC and could relate to error evaluation/detection, as suggested previously (Ursu et al., 2009; Hargreaves et al., 2012). Specifically, the rostral cingulate motor area neighboring primary and supplementary motor areas (Jumah and Dossani, 2022) reportedly engages during the self-detected errors as well as negative feedback (Ullsperger and von Cramon, 2003), supporting the suggested processing sequence.

While these regions fit well into the suggested categorization of error processing into subprocesses, the sequence of engagement in relation to the Euclidean error signal nonetheless raises some questions. For example, RMF, MTG and IN, all areas that best fit error perception or awareness, engage at vastly different periods around the first local maximum of the Euclidean error signal. While RMF and MTG seem to portray the perception of an increasing deviation between target and feedback, the IN engages last in the discussed sequence, coinciding with the perception of increasingly congruent target and feedback information. This observation suggests that the mentioned regions cater to different intricacies of error monitoring. Relating these observations to the reported scalp potentials, another incongruence to our categorization arises. From our observations, the ERN-like complex occurred simultaneously with the cortical activation of regions involved in error perception and evaluation and arose shortly after minima in the Euclidean error signal. However, according to conflict-monitoring theory, one might expect the observed ERN-like potential rather at or shortly after maxima of the Euclidean error signal, where the conflict between target and feedback arguably peaks (Yeung et al., 2004). Instead, the alternating engagement of the regions mentioned before relating to action monitoring, error perception and evaluation rather promotes that our suggested sequence of subprocesses executes at a much faster pace than initially proposed and might indicate that learning, as proposed by the reinforcement-learning theory, is attempted (Holroyd and Coles, 2002).

Finally, within the regarded paradigms, we hypothesize that the cognitive activity related to the correction of erroneous feedback should reach a maximum as the deviation from the intended position peaks. Indeed, the PCC reportedly connects observed outcomes of prior decisions with higher-level strategies (Pearson et al., 2009) and interestingly coincides with the occurrence of the Pe-like scalp potential at the maximum of the Euclidean error signal, which tentatively hints at involvement in correction efforts. However, the lack of usually consulted measures for correction - force or velocity of a collected response signal to the erroneous event, for instance (Carbonnell and Falkenstein, 2006; Burle et al., 2008) - did not allow for a clear statement on behavioral adjustments within this study. As the performance largely depended on the detection capacity of our movement decoders, measures of latency or progress such as the much-employed post-error slowing (Chang et al., 2014) or post-error improvements in accuracy (Carp and Compton, 2009) could not be used. Furthermore, it remains unclear whether the conjunction of the Pe and maxima in the perceived error between target and feedback portrays a causal relationship between the two, or whether the Pe just arises time-locked to the same event provoking the ERN-like component and the time delay coincidentally matches up with local maxima. Latencies of up to 500 ms after an error occurrence have long since been established (Falkenstein et al.), however, our results reveal a temporal distance between supposed ERN and Pe of about 750 ms for able-bodied in both datasets (see Figs. 4A and 7A) and the participant with SCI (Fig. 8A). According to this, our findings suggest that the positivity we observed corresponds to behavioral adjustments, rather than a reaction to the error (initial deviation from the target) itself. The Pe was recently reported as a stand-alone correlate to error awareness that can even appear without the prior occurrence of an ERN (Di Gregorio et al., 2018), supporting the hypothesis that these components of error processing are indeed distinct. However, other research identified the Pe as a correlate to accumulating information about erroneous events (Steinhauser and Yeung, 2010) and confidence in previously made decisions (Boldt and Yeung, 2015; Desender et al., 2019), rather than a correlate to corrective behavior itself as our timeline might suggest. In total, further investigations will need to clarify whether single contributions can be identified in the whole error processing mechanism, or

whether this process constitutes a superposition of various feedback networks.

5. Limitations of our approach

As this work relied on previously recorded data, several issues in need of correction must be mentioned for further studies. First, the tracking tasks we designed leave limited options for disentangling the different components of error processing. All at once, cognitive functions for error monitoring, perception, evaluation, and correction are in demand, which makes a clear evaluation of functional connectivity arduous at best. Previous literature forms the framework for analysis in this case. However, a more specific paradigm design will be needed for future work. Second, the sinusoidal behavior of the target, initially designed to prevent correlation between both Cartesian axes, further obscured the origin of periodicity in the data and required extensive additional analysis to disprove a direct relation between the observed patterns and the target's kinematics (see Fig.S9 and Fig.S10, supplementary material). Dependencies of this kind need to be studied in detail in further studies. And lastly, of course, source space decomposition must be analyzed with caution. While our source space results - especially the regions of interest - are in line with previous works, the spatial resolution of the inverse solution remains an issue, and bold interpretation must be avoided. High-density EEG setups and individual MRI scans alleviate this problem and could further contribute to sound analysis of error processing in the human brain.

6. Conclusions

Most interestingly, we conclude that utilizing a periodically varying error signal instead of established discrete error stimuli (to our knowledge, for the first time) elicits a continuous cognitive response phase-locked to the error signal. This continuous neural correlate exhibited EEG patterns akin to error-related negativity and consecutive error positivity reported within discrete-stimulus tasks and arose exclusively in erroneous feedback conditions. It further proved to be robust to different stimulus types, appearing consistent for both visual and kinesthetic feedback and emerged as independent of the error modality, arising both for error processing during attempted and executed movement. Furthermore, we observed consistent patterns both in the able-bodied and the spinal cord injured participant (AIS A), which, considering the high-level lesion (NLI C2), affirms our findings even for the extreme case of strictly efferent signals. And finally, we were able to tentatively link the periodic behavior of the error-induced modulations in a network of cortical regions to action monitoring, error perception, error evaluation, and corrective behavior, suggesting that identifying single components of the whole error processing mechanism is feasible.

Availability statement

All investigated raw EEG datasets as well as related Matlab scripts are available upon request to the corresponding author and require a formal data sharing agreement.

Declaration of Competing Interest

The authors declare that they have no known competing financial interests or personal relationships that could have appeared to influence the work reported in this paper.

Credit authorship contribution statement

Hannah S. Pulferer: Conceptualization, Methodology, Formal analysis, Investigation, Writing – original draft, Writing – review & editing, Visualization. **Kyriaki Kostoglou:** Methodology, Software, Resources, Formal analysis, Writing – review & editing. **Gernot R. Müller-Putz:** Conceptualization, Writing – review & editing, Supervision, Project administration, Funding acquisition.

Funding

This work was supported by funding from the European Research Council (ERC-CoG 2015 681231 'Feel Your Reach'); NTU-TUG joint Ph.D. program.

Acknowledgments

The authors acknowledge Valeria Mondini, Nitikorn Srisrisawang, Shayan Jalilpour, and Michael Wimmer of the extended Graz BCI Lab for their valuable comments and suggestions on the methodology and interpretation of the data.

Supplementary materials

Supplementary material associated with this article can be found, in the online version, at doi:10.1016/j.neuroimage.2023.120144.

References

Akaike, H., 1974. A new look at the statistical model identification. IEEE Trans. Automat. Contr. 19 (6), 716–723.
Akaike, H., 1998. On the Use of a Linear Model for the Identification of Feedback Systems. In: Statistics. Springer Series, pp. 115–129. doi:10.1007/978-1-4612-1694-0_9.
Althouse, A.D., 2021. Post Hoc power: not empowering, just misleading. J. Surg. Res. A3–A6.
Baccala, L.A., Sameshima, K., Ballester, G., Valle, A.C.d., Yoshimoto, C.E., Timo-Iaria, C., 1998. Studying the interaction between brain structures via directed coherence and a causality test. Appl. Signal Process. 5, 40–48.
Badgaiyan, R.D., Posner, M.I., 1998. Mapping the cingulate cortex in response selection and monitoring. Neuroimage 7 (3), 255–260.
Benjamini, Y., Hochberg, Y., 1995. Controlling the false discovery rate: a practical and powerful approach to multiple testing. J. R. Statist. Soc.. Wiley 57 (1), 289–300.
Boldt, A., Yeung, N., 2015. Shared neural markers of decision confidence and error detection. J. Neurosci. 35 (8), 3478–3484.
Botvinick, M.M., Braver, T.S., Barch, D.M., Carter, C.S., Cohen, J.D., 2001. Conflict monitoring and cognitive control. Psychol. Rev. 108 (3), 624–652.
Brainard, D.H., 1997. The psychophysics toolbox. Spat. Vis. 10 (4), 433–436.
Brown, J.W., Braver, T.S., 2005. Learned predictions of error likelihood in the anterior cingulate cortex. Science 307 (5712), 1118–1121.
Burle, B., Roger, C., Allain, S., Vidal, F., Hasbroucq, T., 2008. Error negativity does not reflect conflict: a reappraisal of conflict monitoring and anterior cingulate cortex activity. J. Cogn. Neurosci. 20 (9), 1637–1655.
Carbonnell, L., Falkenstein, M., 2006. Does the error negativity reflect the degree of response conflict? Brain Res. 1095 (1), 124–130 Elsevier.
Carp, J., Compton, R.J., 2009. Alpha power is influenced by performance errors. Psychophysiology 46 (2), 336–343.
Carter, C.S., Braver, T.S., Barch, D.M., Botvinick, M.M., Noll, D., Cohen, J.D., 1998. Anterior cingulate cortex, error detection, and the online monitoring of performance. Science 280 (5364), 747–749.
Chang, A., Chen, C.-C., Li, H.-H., Li, C.-S.R., 2014. Event-related potentials for post-error and post-conflict slowing. PLoS ONE 9 (6), e99909.
Chen, S., Shu, X., Wang, H., Ding, L., Fu, J., Jia, J., 2021. The differences between motor attempt and motor imagery in brain-computer interface accuracy and event-related desynchronization of patients with hemiplegia. Front. Neurorobot. 15, 706630.
Dehaene, S., Posner, M.I., Tucker, D.M., 1994. Localization of a Neural System for Error Detection and Compensation. Psychol. Sci. 5 (5), 303–305 SAGE Publications Inc.
Delorme, A., Makeig, S., 2004. EEGLAB: an open source toolbox for analysis of single-trial EEG dynamics including independent component analysis. J. Neurosci. Methods 134 (1), 9–21.
Desender, K., Murphy, P., Boldt, A., Verguts, T., Yeung, N., 2019. A Postdecisional neural marker of confidence predicts information-seeking in decision-making. J. Neurosci. 39 (17), 3309–3319.
Desikan, R.S., Ségonne, F., Fischl, B., Quinn, B.T., Dickerson, B.C., Blacker, D., Buckner, R.L., Dale, A.M., Maguire, R.P., Hyman, B.T., Albert, M.S., Killiany, R.J., 2006. An automated labeling system for subdividing the human cerebral cortex on MRI scans into gyral based regions of interest. Neuroimage 31 (3), 968–980.
Di Gregorio, F., Maier, M.E., Steinhauser, M., 2018. Errors can elicit an error positivity in the absence of an error negativity: evidence for independent systems of human error monitoring. Neuroimage 172, 427–436.
Endrass, T., Reuter, B., Kathmann, N., 2007. ERP correlates of conscious error recognition: aware and unaware errors in an antisaccade task. Eur. J. Neurosci. 26 (6), 1714–1720.
Epstein, R., Kanwisher, N., 1998. A cortical representation of the local visual environment. Nature. nature.com. Available at https://www.nature.com/articles/33402?free=2.
Faes, L., Erla, S., Porta, A., Nollo, G., 2013. A framework for assessing frequency domain causality in physiological time series with instantaneous effects. Philos. Trans. A Math. Phys. Eng. Sci. 371 (1997), 20110618.

Faes, L., Porta, A., Nollo, G., 2010. Testing frequency-domain causality in multivariate time series. IEEE Trans. Biomed. Eng. 57 (8), 1897–1906.
Falkenstein, M., 1989. Error processing in choice reaction tasks with focused and cross-modal divided attention. An ERP study. l Conference on EventRelated Potentials of the Brain. May 23-June 3. Noordwijk, the Netherlands.
Falkenstein, M., Hohnsbein, J., Hoormann, J., Blanke, L., 1991. Effects of crossmodal divided attention on late ERP components. II. Error processing in choice reaction tasks. Electroencephalogr. Clin. Neurophysiol. 78 (6), 447–455.
Falkenstein, M., Hoormann, J., Christ, S., Hohnsbein, J., 2000. ERP components on reaction errors and their functional significance: a tutorial. Biol. Psychol. 51 (2–3), 87–107.
Falkenstein, M., Hoormann, J., Christ, S., Hohnsbein, J.,1990. Effects of errors in choice reaction tasks on the ERP under focused and divided attention. In: Brunia, C.H.M., Gaillard, A.W.K., Kok, A. (Eds.), Psychophysiological Brain Research. Tilburg University Press, pp. 192–195.
Frömer, R., Nassar, M.R., Bruckner, R., Stürmer, B., Sommer, W., Yeung, N., 2021. Response-based outcome predictions and confidence regulate feedback processing and learning. eLife 10. doi:10.7554/eLife.62825.
Gehring, W.J., Liu, Y., Orr, J.M., Carp, J., 2012. The Error-Related Negativity (ERN/Ne). The Oxford Handbook of Event-Related Potential Components, 641. Oxford University Press, New York, NY, US, pp. 231–291 xxii.
Gehring, W.J., Goss, B., Coles, M.G.H., Meyer, D.E., Donchin, E., 2018. The error-related negativity. Perspect. Psychol. Sci. 13 (2), 200–204.
Goodman, S.N., Berlin, J.A., 1994. The use of predicted confidence intervals when planning experiments and the misuse of power when interpreting results. Ann. Intern. Med. 121 (3), 200–206.
Gramfort, A., Papadopoulo, T., Olivi, E., Clerc, M., 2010. OpenMEEG: opensource software for quasistatic bioelectromagnetics. Biomed. Eng. Online 9, 45.
Granger, C.W.J., 1969. Investigating causal relations by econometric models and cross-spectral methods. Econometrica 37 (3), 424–438 [Wiley, Econometric Society].
Hampshire, A., Chamberlain, S.R., Monti, M.M., Duncan, J., Owen, A.M., 2010. The role of the right inferior frontal gyrus: inhibition and attentional control. Neuroimage 50 (3), 1313–1319.
Hargreaves, E.L., Mattfeld, A.T., Stark, C.E., Suzuki, W.A., 2012. Conserved fMRI and LFP signals during new associative learning in the human and macaque monkey medial temporal lobe. Neuron 74 (4), 743–752.
Hartwigsen, G., Bestmann, S., Ward, N.S., Woerbel, S., Mastroeni, C., Granert, O., Siebner, H.R., 2012. Left dorsal premotor cortex and supramarginal gyrus complement each other during rapid action reprogramming. J. Neurosci. 32 (46), 16162–16171 a.
van der Helden, J., Boksem, M.A.S., Blom, J.H.G., 2009. The importance of failure: feedback-related negativity predicts motor learning efficiency. Cereb. Cortex 20 (7), 1596–1603 Oxford Academic.
Herrington, J.D., Nymberg, C., Schultz, R.T., 2011. Biological motion task performance predicts superior temporal sulcus activity. Brain Cogn. 77 (3), 372–381 Elsevier.
Herrmann, M.J., Römmler, J., Ehlis, A.C., Heidrich, A., Fallgatter, A.J., 2004. Source localization (LORETA) of the error-related-negativity (ERN/Ne) and positivity (Pe). Brain Res. Cogn. Brain Res. 20 (2), 294–299.
Hester, R., Nestor, L., Garavan, H., 2009. Impaired error awareness and anterior cingulate cortex hypoactivity in chronic cannabis users. Neuropsychopharmacology 34 (11), 2450–2458.
Holroyd, C.B., Coles, M.G.H., 2002. The neural basis of human error processing: reinforcement learning, dopamine, and the error-related negativity. Psychol. Rev. 109 (4), 679–709.
Holroyd, C.B., Dien, J., Coles, M.G., 1998. Error-related scalp potentials elicited by hand and foot movements: evidence for an output-independent error-processing system in humans. Neurosci. Lett. 242 (2), 65–68.
Jumah, F.R., Dossani, R.H., 2022. Neuroanatomy. Cingulate Cortex. StatPearls Publishing.
Keyl, P., Schneiders, M., Schuld, C., Franz, S., Hommelsen, M., Weidner, N., Rupp, R., 2018. Differences in characteristics of error-related potentials between individuals with spinal cord injury and age- and sex-matched able-bodied controls. Front. Neurol. 9, 1192.
Kilintari, M., Raos, V., Savaki, H.E., 2014. Involvement of the superior temporal cortex in action execution and action observation. J. Neurosci. 34 (27), 8999–9011 Soc Neuroscience.
Klein, T.A., Endrass, T., Kathmann, N., Neumann, J., von Cramon, D.Y., Ullsperger, M., 2007. Neural correlates of error awareness. Neuroimage 1774–1781. doi:10.1016/j.neuroimage.2006.11.014.
Kleiner, M., Brainard, D., Pelli, D., 2007. ECVP '07 abstracts,". In: Perception, 36. SAGE Publications, pp. 1–235.
Kobler, R.J., Sburlea, A.I., Mondini, V., Müller-Putz, G.R., 2019. HEAR to remove pops and drifts: the high-variance electrode artifact removal (HEAR) algorithm. In: Proceedings of the 41th Annual International Conference of the IEEE Engineering in Medicine and Biology Society (EMBC). IEEE Xplore.
Kobler, R.J., Sburlea, A.I., Lopes-Dias, C., Schwarz, A., Hirata, M., Müller-Putz, G.R, 2020a. Corneo-retinal-dipole and eyelid-related eye artifacts can be corrected offline and online in electroencephalographic and magnetoencephalographic signals. Neuroimage 218, 117000.
Kobler, R.J., Sburlea, A.I., Mondini, V., Hirata, M., Müller-Putz, G.R., 2020b. Distance- and speed-informed kinematics decoding improves M/EEG based upper-limb movement decoder accuracy. J. Neural. Eng. 17 (5), 056027.
Koelewijn, T., van Schie, H.T., Bekkering, H., Oostenveld, R., Jensen, O., 2008. Motor-cortical beta oscillations are modulated by correctness of observed action. Neuroimage 40 (2), 767–775.
Kostoglou, K., Müller-Putz, G.R., 2021. Directed connectivity analysis in people with spinal cord injury during attempted arm and hand movements. In: Proc. Annual Meeting of the Austrian Society forBiomedical Engineering 2021. Annual Meeting of the Austrian Society for Biomedical Engineering 2021 doi:10.3217/978-3-85125-826-4-20.
Ku, Sp., Hargreaves, E.L., Wirth, S., Suzuki, W.A., 2021. The contributions of entorhinal cortex and hippocampus to error driven learning. Commun. Biol. 4 (1), 618.
Kybic, J., Clerc, M., Faugeras, O., Keriven, R., Papadopoulo, T., 2006. Generalized head models for MEG/EEG: boundary element method beyond nested volumes. Phys. Med. Biol. 51 (5), 1333–1346.
Laurens, C.R., Ngan, E.T., Bates, A.T., Kiehl, K.A., Liddle, P.F., 2003. Rostral anterior cingulate cortex dysfunction during error processing in schizophrenia. Brain doi:10.1093/brain/awg056.
Li, C.R., Huang, C., Constable, R.T., Sinha, R., 2006. Imaging response inhibition in a stop-signal task: neural correlates independent of signal monitoring and post-response processing. J. Neurosci. 26 (1), 186–192.
Lopes-Dias, C., Sburlea, A.I., Breitegger, K., Wyss, D., Drescher, H., Wildburger, R., Müller-Putz, G.R., 2021. Online asynchronous detection of error-related potentials in participants with a spinal cord injury using a generic classifier. J. Neural. Eng. 046022. doi:10.1088/1741-2552/abd1eb.
Lopes-Dias, C., Sburlea, A.I., Müller-Putz, G.R., 2018. Masked and unmasked error-related potentials during continuous control and feedback. J. Neural. Eng. 15 (3), 036031 IOP Publishing.
Lourenco, F., Casey, B.J., 2013. Adjusting behavior to changing environmental demands with development. Neurosci. Biobehav. Rev. 37 (9 Pt B), 2233–2242.
Martinez-Cagigal, V., Kobler, R.J., Mondini, V., Hornero, R., Müller-Putz, G.R., 2020. Non–linear online low-frequency EEG decoding ofarm movements during a pursuit tracking task. In: 2020 42nd Annual International Conference of the IEEE Engineering in Medicine Biology Society (EMBC), pp. 2981–2985.
Mathewson, K.J., Dywan, J., Segalowitz, S.J., 2005. Brain bases of error-related ERPs as influenced by age and task. Biol. Psychol. 70 (2), 88–104 Elsevier.
Maynard Jr., F.M., Bracken, M.B., Creasey, G., Ditunno Jr., J.F., Donovan, W.H., Ducker, T.B., Garber, S.L., Marino, R.J., Stover, S.L., Tator, C.H., Waters, R.L., Wilberger, J.E., Young, W., 1997. International standards for neurological and functional classification of spinal cord injury. Spinal Cord 35 (5), 266–274.
Miltner, W.H.R., Braun, C.H., Coles, M.G.H., 1997. Event-related brain potentials following incorrect feedback in a time-estimation task: evidence for a 'Generic' neural system for error detection. J. Cogn. Neurosci. 9 (6), 788–798.
Mondini, V., Kobler, R.J., Sburlea, A.I., Müller-Putz, G.R., 2020. Continuous low-frequency EEG decoding of arm movement for closed-loop, natural control of a robotic arm. J. Neural Eng. 17 (4), 046031.
Müller-Putz, G.R., Schwarz, A., Pereira, J., Ofner, P., 2016. From classic motor imagery to complex movement intention decoding: the noninvasive Graz-BCI approach. Prog. Brain Res. 228, 39–70.
Müller-Putz, G.R., Kobler, R.J., Pereira, J., Lopes-Dias, C., Hehenberger, L., Mondini, V., Martínez-Cagigal, V., Srisrisawang, N., Pulferer, H., Batistić, L., Sburlea, A.I., 2022. Feel Your Reach: an EEG-based framework to continuously detect goal-directed movements and error processing to gate kinesthetic feedback informed artificial arm control. Front. Hum. Neurosci. 110 Frontiers.
Mulliken, G.H., Musallam, S., Andersen, R.A., 2008. Decoding trajectories from posterior parietal cortex ensembles. J. Neurosci. 28 (48), 12913–12926.
Nieuwenhuis, S., Ridderinkhof, K.R., Blom, J., Band, G.P.H., Kok, A., 2001. Error-related brain potentials are differentially related to awareness of response errors: evidence from an antisaccade task. Psychophysiology 38 (5), 752–760.
Nieuwenhuis, S., Ridderinkhof, K.R., Talsma, D., Coles, M.G.H., Holroyd, C.B., Kok, A., van der Molen, M.W., 2002. A computational account of altered error processing in older age: dopamine and the error-related negativity. Cogn. Affect. Behav. Neurosci. 2 (1), 19–36.
Nieuwenhuis, S., Holroyd, C.B., Mol, N., Coles, M.G.H, 2004. Reinforcement-related brain potentials from medial frontal cortex: origins and functional significance. Neuroscience and Biobehavioral Reviews 28 (4), 441–448.
Ofner, P., Schwarz, A., Pereira, J., Müller-Putz, G.R., 2017. Upper limb movements can be decoded from the time-domain of low-frequency EEG. PLoS ONE 12 (8), e0182578.
Oldfield, R.C., 1971. The assessment and analysis of handedness: the Edinburgh inventory. Neuropsychologia 97–113. doi:10.1016/0028-3932(71)90067-4.
Olvet, D.M., Hajcak, G., 2008. The error-related negativity (ERN) and psychopathology: toward an endophenotype. Clin. Psychol. Rev. 28 (8), 1343–1354 Elsevier.
Pail, M., Dufková, P., Mareček, R., Zelinková, J., Mikl, M., Shaw, D.J., Brázdil, M., 2016. Connectivity of superior temporal sulcus during target detection. Journal of psychophysiology 30 (1), 29–37.
Pascual-Marqui, R.D., 2002. Standardized low-resolution brain electromagnetic tomography (sLORETA): technical details. Methods Find Exp. Clin. Pharmacol. 24 (Suppl D), 5–12.
Pearson, J.M., Hayden, B.Y., Raghavachari, S., Platt, M.L., 2009. Neurons in posterior cingulate cortex signal exploratory decisions in a dynamic multioption choice task. Curr. Biol. 19 (18), 1532–1537.
Pelli, D.G., 1997. The VideoToolbox software for visual psychophysics: transforming numbers into movies. Spat. Vis. 10 (4), 437–442 Brill.
Pulferer, H.S., Ásgeirsdóttir, B., Mondini, V., Sburlea, A.I., Müller-Putz, G.R., 2022. Continuous 2D trajectory decoding from attempted movement: across-session performance in able-bodied and feasibility in a spinal cord injured participant. J. Neural. Eng. IOP Publishing doi:10.1088/1741-2552/ac689f.
Pulferer, H.S., Müller-Putz, G.R., 2022. Continuous error processing during a closed-loop 2D tracking task. Curr. Direct. Biomed. Eng. 8 (2), 173–176 De Gruyter.
Rabbitt, P.M., 1966. Errors and error correction in choice-response tasks. J. Exp. Psychol. 71 (2), 264–272.
Saito, Y., Harashima, H., 1981. Tracking of information within multichannel EEG record causal analysis in eeg. In: Yamaguchi, N, Fujisawa, K (Eds.), Recent Advances in ${EEG} and {EMG}$ Data Processing. Elsevier.

Schlögl, A., 2006. A comparison of multivariate autoregressive estimators. Signal Processing 86 (9), 2426–2429.
Schneider, T., Neumaier, A., 2001. Algorithm 808: aRfit—A matlab package for the estimation of parameters and eigenmodes of multivariate autoregressive models. ACM Trans. Math. Softw. 27 (1), 58–65 Association for Computing Machinery. New York, NY, USA: Association for Computing Machinery.
Seeber, M., Scherer, R., Wagner, J., Solis-Escalante, T., Müller-Putz, G.R., 2015. High and low gamma EEG oscillations in central sensorimotor areas are conversely modulated during the human gait cycle. Neuroimage 112, 318–326.
Spüler, M., Niethammer, C., 2015. Error-related potentials during continuous feedback: using EEG to detect errors of different type and severity. Front. Hum. Neurosci. 9, 155.
Srisrisawang, N., Müller-Putz, G.R., 2022. Applying dimensionality reduction techniques in source-space electroencephalography via template and magnetic resonance imaging-derived head models to continuously decode hand trajectories. Front. Hum. Neurosci. 16, 830221.
Steinhauser, M., Yeung, N., 2010. Decision processes in human performance monitoring. J. Neurosci. 30 (46), 15643–15653.
Swick, D., Ashley, V., Turken, A.U., 2008. Left inferior frontal gyrus is critical for response inhibition. BMC Neurosci. 9, 102.
Tadel, F., Baillet, S., Mosher, J.C., Pantazis, D., Leahy, R.M., 2011. Brainstorm: a user-friendly application for MEG/EEG analysis. Comput. Intell. Neurosci. 2011, 879716.
Tadel, F., Bock, E., Niso, G., Mosher, J.C., Cousineau, M., Pantazis, D., Leahy, R.M., Baillet, S., 2019. MEG/EEG group analysis with brainstorm. Front. Neurosci. 13, 76.
Turken, A.U., Swick, D, 2008. The effect of orbitofrontal lesions on the error-related negativity. Neurosci. Lett. 441 (1), 7–10.
Ullsperger, M., von Cramon, D.Y., 2003. Error monitoring using external feedback: specific roles of the habenular complex, the reward system, and the cingulate motor area revealed by functional magnetic resonance imaging. J. Neurosci. 23 (10), 4308–4314 Society for Neuroscience.
Ullsperger, M., Danielmeier, C., Jocham, G., 2014. Neurophysiology of performance monitoring and adaptive behavior. Physiol. Rev. 94 (1), 35–79.
Ullsperger, M., Szymanowski, F., 2004. ERP correlates of error relevance. In: Errors, Conflicts, and the Brain: Current Opinions On Performance Monitoring. MPI for Human Cognitive and Brain Sciences, pp. 171–177.
Ursu, S., Clark, K.A., Aizenstein, H.J., Stenger, V.A., Carter, C.S., 2009. Conflict-related activity in the caudal anterior cingulate cortex in the absence of awareness. Biological Psychology 80 (3), 279–286.
Van 't Ent, D., Apkarian, P., 1999. Motoric response inhibition in finger movement and saccadic eye movement: a comparative study. Clin. Neurophysiol. 110 (6), 1058–1072.
Völker, M., Fiederer, L.D.J., Berberich, S., Hammer, J., Behncke, J., Kršek, P., Tomášek, M., Marusič, P., Reinacher, P.C., Coenen, V.A, Helias, M., Schulze-Bonhage, A., Burgard, W., Ball, T., 2018. The dynamics of error processing in the human brain as reflected by high-gamma activity in noninvasive and intracranial EEG. Neuroimage 173, 564–579.
Wenderoth, N., Debaere, F., Sunaert, S., Swinnen, S.P., 2005. The role of anterior cingulate cortex and precuneus in the coordination of motor behaviour. Eur. J. Neurosci. 22 (1), 235–246.
Wimmer, M., Kostoglou, K., Müller-Putz, G.R., 2022. Measuring spinal cord potentials and cortico-spinal interactions after wrist movements induced by neuromuscular electrical stimulation. Front. Hum. Neurosci. 16, 858873.
Worsley, K.J., Taylor, J.E., Carbonell, F., Chung, M.K., Duerden, E., Bernhardt, B., Lyttelton, O.C., Boucher, M., Evans, A.C., 2009. SurfStat: A Matlab toolbox for the statistical analysis of univariate and multivariate surface and volumetric data using linear mixed effects models and random field theory. NeuroImage 47.
Yeung, N., Bogacz, R., Holroyd, C.B., Cohen, J.D., 2004a. Detection of synchronized oscillations in the electroencephalogram: an evaluation of methods. Psychophysiology 41 (6), 822–832.
Yeung, N., Botvinick, M.M., Cohen, J.D., 2004b. The neural basis of error detection: conflict monitoring and the error-related negativity. Psychol. Rev. 111 (4), 931–959 American Psychological Association (APA).
Yordanova, J., Falkenstein, M., Hohnsbein, J., Kolev, V., 2004. Parallel systems of error processing in the brain. Neuroimage 22 (2), 590–602.